STARS

Electronic Theses and Dissertations, 2004-2019

2015

Functional Characterization of Green Sorption Media and Scaling of Pilot Studies for Copper Removal in Stormwater Runoff

Cameron Houmann
University of Central Florida

Part of the Civil Engineering Commons, and the Water Resource Management Commons

Find similar works at: https://stars.library.ucf.edu/etd

University of Central Florida Libraries http://library.ucf.edu

FUNCTIONAL CHARACTERIZATION OF GREEN SORPTION MEDIA AND SCALING OF PILOT STUDIES FOR COPPER REMOVAL IN STORMWATER RUNOFF

by

CAMERON HOUMANN
B.Sc. Walla Walla University, 2013

A thesis submitted for the partial fulfillment of the requirements
for the degree of Master of Science
in the Department of Civil, Environmental, and Construction Engineering
in the College of Engineering and Computer Science
at the University of Central Florida
Orlando, Florida

Spring Term
2015

Major Professor: Ni-Bin Chang

ABSTRACT

Green adsorption media with the inclusion of renewable and recycled materials can be applied as a stormwater best management practice for copper removal. A green adsorption media mixture composed of recycled tire chunk, expanded clay aggregate, and coconut coir was physicochemically evaluated for its potential use in an upflow media filter. The results found that the use of the green adsorption media mixture in isolation or the coconut coir with an expanded clay filtration chamber could be an effective and reliable stormwater best management practice for copper removal. A suite of tests were conducted on the media mixture and the individual media components including studies of isotherm, reaction kinetics, column adsorption and reaction kinetics. Batch adsorption tests revealed that the media and media mixture follow both the Freundlich and Langmuir isotherm models and that the coconut coir had the highest affinity for copper. A screening of desorbing agents revealed that hydrochloric acid has good potential for copper desorption, while batch tests for desorption with hydrochloric acid as the desorbing agent showed the data fit the Freundlich isotherm model. Reaction kinetics revealed that the adsorption reaction took less than 1 hour to reach equilibrium and that it followed pseudo-second order kinetics for the mixture and coconut. Desorption kinetic data had high correlation with the pseudo-second order model and revealed a rapid desorption reaction. Batch equilibrium data over 3 adsorption/desorption cycles found that the coconut coir and media mixture were the most resilient and demonstrated that they could be used through 3 or more adsorption/desorption cycles. The coconut coir also performed the best under dynamic conditions, having an equilibrium uptake of 1.63 mg·g^{-1}, compared to 0.021 mg·g^{-1} at an influent concentration of 1.0 mg·L^{-1} and a hydraulic retention time of 30 minutes. A physical evaluation of the media found the macro-scale properties, such as particle size distribution and mass-volume relationships, and observed the micro-scale properties such as surface and pore microstructures, crystalline structures, and elemental composition. FE-SEM imaging found a strong correlation between

iii

the porosity of the micro pore structure and the adsorptive capacity. The equilibrium and dynamic adsorption testing results were confirmed by elemental analysis, which showed measureable quantities of copper in the coconut coir and media mixture after adsorption followed by partial desorption. A new scaling-up theory was developed through a joint consideration of the Damköhler and Péclet numbers for a constant media particle size such that a balance between transport-controlled and reaction-controlled kinetics can be harmonized. A series of column breakthrough tests at varying hydraulic residence times revealed a clear peak adsorptive capacity for the media mixture at a Damköhler number of 2.7. The Péclet numbers for the column breakthrough tests indicated that mechanical dispersion is an important effect that requires further consideration in the scaling-up process. However, perfect similitude of the Damköhler number cannot be maintained for a constant media particle size, and relaxation of hydrodynamic similitude through variation of the Péclet number must occur.

ACKNOWLEDGMENTS

TABLE OF CONTENTS

LIST OF FIGURES

LIST OF TABLES

CHAPTER 1:   INTRODUCTION

1.1. <u>Ecological Effects of Excess Copper in Aquatic Environments</u>

Copper is a pollutant of concern in stormwater runoff due to its toxic effects on aquatic ecosystems, its non-biodegradable nature, and its ability to accumulate in sediments and tissues of living organisms. It is toxic as a free ion to aquatic invertebrates, such as snails and zooplankton, and is toxic to fish at a low pH. In particular, salmonoids are intolerant to dissolved copper, with 96-hour LC50 between 17 and 38 $\mu g \cdot L^{-1}$ (Chapman, 1978). Bacteria living in nitrogen-removing biofilms are especially susceptible, as exposure to copper has been shown to change the structure, metabolism, and physiology of biofilms (Barranguet *et al*., 2002, Boivin *et al*., 2005). In stormwater wet detention ponds, destruction of these communities can decrease the nitrogen-removal efficiency through the elimination of nitrifying and denitrifying bacteria (Jones, 2013). As a result, excess copper loading is a concern in both the natural and built environment.

In surface water bodies that suffer from severe algal growth, copper sulfate ($CuSO_4$), also known as bluestone or blue powder, is a commonly applied copper-based algaecide. Due to the high required doses, ranging from 0.3 $mg \cdot L^{-1}$ to 2.0 $mg \cdot L^{-1}$ (Nor, 1987), copper sulfate application results in large spikes of copper concentration in stormwater wet detention ponds. However, application of $CuSO_4$ can be lethal to a range of non-target organisms. The necessary dose required to kill algae was found to be 10 to 100 times the amount that is lethal to zooplankton, a natural consumer of algae (Cooke and Kennedy, 2001). $CuSO_4$ application causes only a temporary spike, as copper concentrations in the water column were found to return to pre-application levels in only 2 hours after an application density of 0.2 Cu^{2+}/m^2 (Button, 1977), accumulating in the sediment instead.

1.2. Sources of Copper in Stormwater Runoff

Impairment due to excessive copper levels is a threat facing a large number of water bodies in the United States. According to the United States Environmental Protection Agency, 844 water bodies nationwide are listed on its impaired water list whose cause of impairment is copper (USEPA, 2014). This includes 12,800 miles of rivers, canals, and streams, 38,558 acres of lakes, ponds, and reservoirs, 987 square miles of bays and estuaries, and 52 miles of coastline. The summary in Table 1.1 illustrates the distribution of copper-impaired water bodies throughout the United States by region. While point-source discharges such as industrial waste and municipal sewage have historically been the culprit of copper pollution, intense government regulation and advances in waste stream treatment technology have limited their impact in waters of developed nations. As a result, discharges from non-point sources have become the major contributor of anthropogenic copper input, as shown in Table 1.2 for the United States.

Table 1.1. Regional distribution of copper-impaired water bodies in the United States

EPA Region	No. Of Impaired Water Bodies
1 - New England	49
2 - New York, New Jersey, Puerto Rico	75
3 - Mid-Atlantic	8
4 - Southeast	185
5 - Great Lakes	34
6 - South Central	56
7 - Midwest	162
8 - Mountains and Prairies	131
9 – Pacific Southwest	122
10 – Pacific Northwest	22

Table 1.2. Contributing sources of copper contamination for impaired water bodies of the United States. Percentages are listed in terms of the total water bodies with identified pollution sources.

Dominant Copper Contamination Source	Percent of Impaired Water Bodies Affected
Mining Activities	34%
Urban Stormwater Runoff	24%
Industrial Discharge	16%
Municipal Discharge	9%
Natural Sources	6%
Historical Pollution	6%
Land Application/Waste Sites/Tanks	3%
Agriculture	1%
Other	1%

A number of studies have discovered high levels of copper exist in stormwater runoff from both urban (Dean et al., 2005, Hilliges *et al*., 2013, Kayhanian *et al*., 2003, Nason *et al*., 2012) and agricultural (Dietrich and Gallagher, 2002, Flores-Vélez *et al*., 1996, Graves *et al*., 2004) settings. Contributing sources of copper in urban stormwater runoff include wood siding treated with CCA (copper, chromium, arsenic), copper gutters, copper pipes, and copper roofing. Runoff from roadways may include copper from break wear and vehicle exhaust. Davis *et* al. (2001) showed that break wear is the leading contributor to copper in urban stormwater runoff and has been estimated to be 75 µg·km^{-1} per vehicle.

Studies in Florida have found that the use of copper as a fungicide and soil amendment can contribute to copper loadings via runoff from agricultural lands (Zhang *et al*., 2003), golf courses (Graves *et al*., 2004), and desorption of accumulated copper on agricultural lands inundated by floods (Hoang *et al*., 2009). Additionally, the use of copper sulfate as an algaecide in manmade wet-detention ponds is common due to the fact that it is water soluble and readily permeates through the water column.

Impairment due to excessive copper levels is a threat facing a large number of water bodies in the United States today. According to the United States Environmental Protection Agency (USEPA), 844

water bodies nationwide are listed on its impaired water list whose cause of impairment is copper (USEPA, 2014). Notably, the majority of the cases, 60%, are believed to be caused by non-point stormwater runoff from urban, agricultural, and mining lands. Under the Clean Water Act, administered by the USEPA, impaired water bodies are required to develop total maximum daily loads (TMDL) for their causes of impairment, which includes load allocations for non-point sources. As a result, there is a need for the development of stormwater best management practices (BMPs) for the control of copper in stormwater management systems to meet TMDL requirements and reduce the anthropogenic copper input to water bodies.

1.3. Use of Green Sorption Media for Copper Removal

Employing a copper-removing sorption media in a fixed-bed filter is a BMP that can be used to reduce copper levels in the water column and sediments of stormwater wet detention ponds. Circulation of water through the sorption media reactor could provide aqueous copper removal via physical adsorption, and a variety of chemical processes such as ion exchange, complexation, and surface micro-precipitation. Circulation through the reactor could be provided continuously or on an event-basis, such as during periods of copper sulfate application or after storm events.

The use of adsorptive media for copper removal in industrial and municipal waste streams has found to be effective and has resulted in a great volume of research. More specifically, many researchers have conducted studies on "green" sorption media, defined here as being comprised of renewable, recycled, or locally-sourced materials. Materials in these studies include, but are not limited to, peat moss (DeBusk *et al*., 1997;, Clark *et al*., 2001), wollastonite (DeBusk *et al*., 1997), crushed limerock (DeBusk, *et al*., 1997), generic hardwood mulch (Ray *et al*., 2006), sawdust from cedar (Djeribi and Hamadoui, 2008) and maple trees (Yu *et al*., 2001), sugar beet pulp (Huguenot *et al*., 2010; Pehlivan *et al*., 2006), fly

ash, corncob and corncob char (Huguenot *et al*., 2010), tea processing waste (Amarasinghe and Williams, 2007; Cay *et al.*, 2004), green algae (Deng *et al.*, 2006), brown seaweed (Antunes *et al*., 2003), sour orange residue (Khormaei *et al.*, 2007) lentil shell, wheat shell, and rice shell (Aydin *et al.*, 2008). The key variables found in these studies to affect copper adsorption include pH, contact time or hydraulic residence time (HRT), and sorbent concentration. Although many of these materials have a high sorption capacity for copper, their applicability as a stormwater BMP has to be further evaluated in terms of the optimal combination of materials to form a unique recipe for treatment.

1.4. **Scope of Research**

The broad objective of this research effort is to evaluate the potential of a green sorption media mixture as a stormwater BMP for copper removal. The media mixture under evaluation consists of 1/3 recycled tire chunk, 1/3 expanded clay aggregate, and 1/3 coconut coir. media composition was developed by Jones (2013) through a screening of green materials, both previously studied in the literature and not yet studied. The materials were considered "green" by being either renewable or recycled materials. The criteria used in this screening consisted of 1.) removal efficiency from published studies, 2.) available surface area for sorption, 3.) particle size, to avoid clogging, 4.) cost. 5.) availability in Florida, and 6.) additional benefits. By considering all of these factors, the media mixture is unique and significant in that it presents a low-cost, renewable media designed specifically for an application in stormwater treatment.

The research work is broken into 3 portions, which are the investigation of the sorption and desorption processes and performance (Chapter 2), a physical characterization of the media at the macro-, meso- and micro-scales (Chapter 3), and the development of a method for scaling pilot studies to field implementations (Chapter 4). Throughout these chapters, this study aims to answer a number of science

questions. First, what are the copper adsorption capacities of the sorption media mixture and individual media components (Chapter 2)? Second, how do the adsorptive characteristics of the media affect the shape of the breakthrough curve and the life expectancy of the media (Chapter 2)? Third, what is the potential for copper removal and recovery from spent media using strong acids as a desorbing agent (Chapter 2)? Fourth, how does the adsorptive capacity of the sorption media vary through multiple adsorption/desorption cycles (Chapter 2)? Fifth, what are the physical characteristics of the sorption media and how do these affect the adsorption and desorption processes (Chapter 3)? Sixth, is the flow regime under the experimental conditions primarily transport-controlled or reaction-controlled (Chapter 4)? Finally, seventh, how can the use of dimensionless numbers for reactive transport be used for optimizing sorption media reactor design at the field scale (Chapter 4)? From these questions, it is hypothesized that 1.) the coconut coir will exhibit the highest adsorption capacity and longest life expectancy which results from a high amount of surface area and an extensive inner pore structure; 2.) desorption with the use of strong acids can extend the life expectancy of the coconut coir beyond 1 usage cycle, and 3.) the peak adsorption capacity of the media can be realized when the reactive transport and advective transport rates are near equal.

The work presented in the following sections will answer these key questions through a series of objectives. Chapter 2 examines the adsorption of copper under equilibrium and dynamic conditions for the media mixture and its individual components, determines the key engineering design variables such as reaction rate and adsorption capacity, estimates the life expectancy of the green sorption media in a reactor, evaluates the desorption of copper under equilibrium for the media and its individual components using desorbing agents, and investigates of the resiliency of the media through multiple adsorption-desorption cycles. Chapter 3 presents the physical characteristics of the media that are key to reactor design at the macro scale, the elemental composition of the media, and a spectroscopic analysis of the media before and after adsorption and desorption to provide support to the conclusions in Chapter 2.

6

Finally, Chapter 4 develops a relationship between the dimensionless numbers for reactive transport and the removal efficiency of the media under dynamic conditions, leading to the development of a new scaling method using these dimensionless numbers.
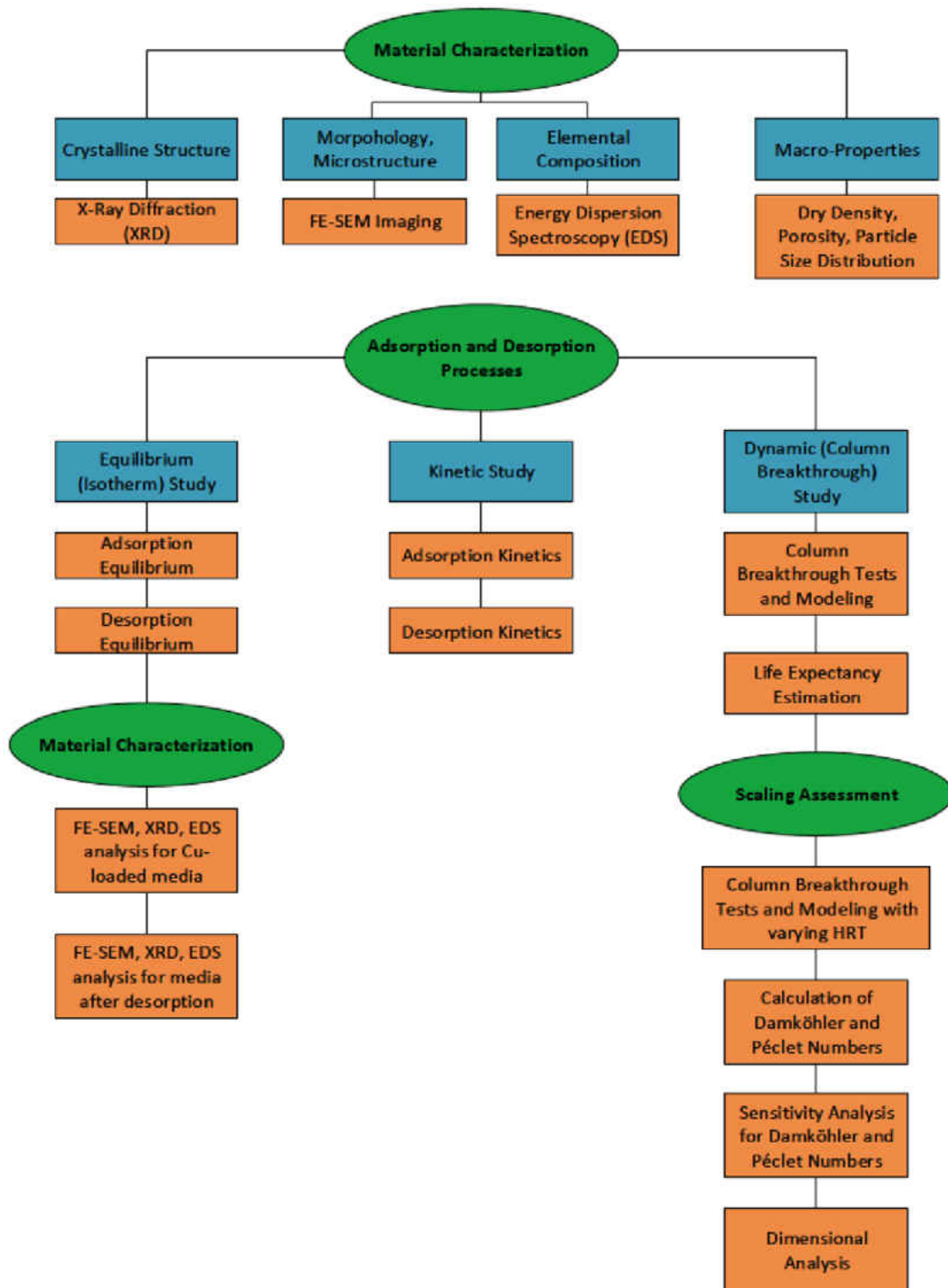
Figure 1.1. Flow chart for the experimental work and analysis

8

1.5. <u>References</u>

Amarasinghe, B.M.W.P.K., and R.A.Williams. 2007. Tea waste as a low cost adsorbent for the removal of Cu and Pb from wastewater. *Chemical Engineering J.* 132: 299–309.

Antunes, W.M., Luna, A.S., Henriques, C.A., and A.C.A. Costa. 2003. An evaluation of copper biosorption by a brown seaweed under optimized conditions. *Electronic J. of Biotechnol*.6: 174–184.

Aydin, H., Bulut, Y., and C. Yerlikaya. 2008. Removal of copper (II) from aqueous solution by adsorption onto low-cost adsorbents. *J. of Environmental Management* 87: 37–45.

Barranguet, C., Plans, M., Van der Grinten, T., Sinke, J.J., and W. Admiraal. 2002. Development of photosynthetic biofilms affected by dissolved and sorbed copper in a eutrophic river. *Environ. Toxicology and Chem.* 21: 1955-1965.

Boivin, M., Massieux, B., Breure, A.M., Van den Ende, F.P., Greve, G.D., Rutgers, M., and W. Admiraal. 2005. Effects of copper and temperature on aquatic bacterial communities. *Aquatic Toxicology* 71: 345-356.

Button, K.S. 1977. Copper dispersal in a water-supply reservoir. *Water Res.* 11: 539-544.

Cay, S., Uyanik, A., and A. Ozasik. 2004. Single and binary component adsorption of copper(II) and cadmium(II) from aqueous solutions using tea-industry waste. *Sep.and Purif. Technology* 38: 273–280.

Chapman, G.A. 1978, Toxicities of Cadmium, Copper, and Zinc to Four Juvenile Stages of Chinook Salmon and Steelhead. *Transactions of the American Fisheries Soc* 107: 841-847.

Clark, S., Pitt, R., and D. Brown. 2001. Effect of anaerbiosis on filter media pollutant retention. *Presented at the Engineering Foundation and American Society of Civil Engineers conference on*

information and monitoring needs for evaluating the mitigation effects of BMPs, Snowmass, Colorado.

Cooke, G., and R. Kennedy. 2001. Managing drinking water supplies. *Lake and Reserv. Management* 17: 157-174.

Davis, A.P., Shokouhian, M., and S. Ni. 2001. Loading estimates of lead, copper, cadmium, and zinc in urban runoff from specific sources. *Chemosphere* 44: 997-1009.

Dean, C.M., Sansalone, J.J., Cartledge, F.K., and J.H. Pardue. 2005. Influence of hydrology on rainfall-runoff metal element speciation. *J. of Environmental Engineering* 131: 632-642.

DeBusk, T.A., Langston, M.A., Schwegler, B.R. and S. Davidson. 1997. An evaluation of filter media for treating stormwater runoff. *Proceedings of the fifth biennial storm water research conference,* hosted by the South Florida Water Management District at the Four Points Sheraton Hotel, West Palm Beach, Florida: 82-89.

Deng, L., Su, Y., Su, H., Wang, X., and X. Zhu. 2006. Biosorption of copper (II) and lead (II) from aqueous solutions by nonliving green algae *Cladophora fascicularis*: equilibrium, kinetics and environmental effects. *Adsorption* 12: 267–277.

Djeribi, R., and O. Hamdaoui. 2008. Sorption of copper(II) from aqueous solutions by cedar sawdust and crushed brick. *Desalination* 225: 95–112.

Dietrich, A.M., and D.L. Gallagher. 2002. Fate and environmental impact of pesticides in plastic mulch production runoff: Field and laboratory studies. *J. of Agricultural and Food Chemistry* 50: 4409-4416.

Flores-Vélez, L.M., Ducaroir, J., Jaunet, A.M., and M. Robert. 1996. Study of the distribution of copper in an acid sandy vineyard soil by three different methods. *European J. of Soil Science* 47: 523-532.

Graves, G.A., Wan, Y., and D. Fike. 2004. Water quality characteristics of storm water from major land uses in South Florida. *J. of the American Water Resources Assoc.* (JAWRA) 40: 1405-1419.

Hilliges, R., Schriewer, A., and B. Helmreich. 2013. A three-stage treatment system for highly polluted urban road runoff. *J. of Environmental Management* 128: 306-312.

Huguenot, D., Bois, P., Jezequel, K., Cornu, J.Y., and T. Lebeau. 2010. Selection of low cost materials for the sorption of copper and herbicides as single or mixed compounds in increasing complexity matrices. *J. Hazard. Mater*. 182: 18-26.

Jones, J. 2013. Chemophysical characteristics and application of biosorption activated media (BAM) for copper and nutrient removal in stormwater management. Thesis, University of Central Florida.

Kayhanian, M., Singh, A., Suverkropp, C., and S. Borroum. 2003. Impact of annual average daily traffic on highway runoff pollutant concentrations. *J. of Environmental Engineering* 129: 975-990.

Khormaei, M., Nasernejad, B., Edrisi, M., and T. Eslamzadeh. 2007. Copper biosorption from aqueous solutions by sour orange residue. *J. of Hazard.Mater.* 149: 269–274.

Nason, J.A., Bloomquist, D.J., and M.S. Sprick. 2012. Factors influencing dissolved copper concentrations in Oregon highway storm water runoff. *J. of Environmental Engineering* 138: 734-742.

Nor, Y.M.. 1987. Ecotoxicity of copper to aquatic biota. *J. Environ. Res*. 43: 274-282.

Pehlivan, E., Cetin, S., and B.H. Yanik. 2006. Equilibrium studies for the sorption of zinc and copper from aqueous solutions using sugar beet pulp and fly ash. *J. Hazard. Mater.* 125: 193-199.

Ray, A.B., Selvakumar, A., and A.N. Tafuri. 2006. Removal of selected pollutants from aqueous media by hardwood mulch. *J. Hazard. Mater.* 136: 213-218.

United States Environmental Protection Agency (USEPA), "Water quality assessment and total maximum daily loads information", http://www.epa.gov/waters/ir/index.html, accessed August 12, 2014.

Yu, B., Zhang, Y., Shukla, A., Shyam, S., and K. Dorris. 2001. The removal of heavy metal from aqueous solutions by sawdust adsorption: removal of lead and its comparison of its adsorption with copper. *J. Hazard. Mater*. 84: 83-94.

Zhang, M., He, Z., Calvert, D., Stofella, P., and X. Yang. 2003. Surface runoff losses of copper and zinc in sandy soils. *J. of Environmental Quality* 032: 909-916.

CHAPTER 2:   ADSORPTION-DESORPTION PROCESSES

2.1. <u>Introduction</u>

2.1.1.   <u>Introduction and Literature Review</u>

Employing a copper-removing sorption media in a fixed-bed filter is a best management practice (BMP) that can be used to reduce copper levels in the water column and sediments of stormwater detention ponds. Removal of metal ions using sorption media is accomplished by a variety of mechanisms, including physical adsorption, ion exchange, complexation, and surface micro-precipitation (Pehlivan *et al*., 2006). In this study, a green sorption media mixture of expanded clay, coconut coir, and tire chunk was investigated for its copper adsorption and desorption characteristics. The media mixture is considered a "green" mixture due to the inclusion of locally-sourced, i.e. expanded clay aggregate and tire material, and recycled material, i.e. recycled coconut waste and tire material. A number of studies on copper adsorption to green sorption media have found a number of effective adsorbents (Table 2.1). Previous studies have shown that in clay-type materials, copper sorption occurs through electrostatic attraction and ion exchange in (Musso *et al*., 2014), through a combination of ion exchange with hydroxyl and carboxylic functional groups and electrostatic attraction in coconut coir (Acheampong *et al*., 2011), and primarily through ion exchange for tire rubber (Calisir *et al*., 2009).

Table 2.1. Summary of recent studies on copper adsorption to green sorption media.

Green Sorption Media	Reference	Operational Conditions		q_{max}
		pH	T (°C)	(mg·g^{-1})
Brown Seaweed	Anutes *et al.*, 2003	5.0	25-55	82.6 - 93.9
Cedar Sawdust	Djeribi and Hamadoui, 2008	5-6	25-45	294.12 -106.38
Coconut Husk	Acheampong *et al.*, 2011	7.0	30	4.62
Coconut Shell	Acheampong *et al.*, 2011	7.0	30	4.21
Fly Ash	Pehlivan *et al.*, 2006	5.5	25	11.43
Green Algae	Deng *et al.*, 2006	5.0	15-45	102.55 - 102.97
Lentil Shell	Aydin *et al.*, 2008	6.0	20-60	8.98 - 9.59
Maple Sawdust	Yu *et al.*, 2001	7.0	23	1.79
Rice Shell	Aydin *et al.*, 2008	6.0	20-60	1.85 - 2.95
Sour Orange Residue	Khormaei *et al*, 2007	4.5	28	52.08
Sugar Beet Pulp	Pehlivan *et al.*, 2006	5.5	25	0.152
	Hugeunot *et al.*, 2010.	4.8	20	17.1
Tea Processing Waste	Amarasinghe and Williams, 2007	5-6	22	48.0
Tire Rubber	Calisir *et al.*, 2009	6.0	25	1.51
Wheat Shell	Aydin *et al.*, 2008	6.0	20-60	7.39 - 17.42

Once the filter media has reached its adsorptive capacity, it must be replaced and the spent media may need to be disposed as a hazardous waste. However, desorption and recovery of the sorbed copper can regenerate the sorption sites on the media so that it may be reused for additional cycles. Desorption of sorbed copper can be achieved through the use of various desorbing agents, primarily acids (Njikam and Schiewer, 2012, Singh *et al*, 2008, Vilar *et al*, 2006) and complexing agents (Njikam and Schiewer, 2012, Singh *et al*, 2008), whose effectiveness may vary between media types, depending on the sorption mechanism involved. Regeneration of the media's sorption sites and recovery of the sorbed copper are

important in establishing the media as a cost-effective and sustainable solution for copper removal in stormwater runoff.

Studies of heavy metal desorption from both green sorption media and inorganic sorption media have mostly mirrored that of adsorption, as the two mechanisms are similar (Vilar *et al*., 2006). Adsorption isotherm equations have been successfully applied to describe equilibrium desorption data, including Langmuir and Freundlich isotherms (Cox *et al*., 1997, Febrianto *et al*., 2008, Piwowarczyk and Holden, 2011, Wang *et al*, 2013), while some mechanistic desorption equilibrium models have been developed (Kyzas *et al*., 2014, Vilar *et al*., 2006). Desorption kinetics have been shown to follow Lagergren pseudo first- and second-order kinetics (Kyzas *et al*., 2014, Njikam and Schiewer, 2012, Singh *et al*., 2008), by assuming that the rate of desorption is proportional to the number of metal-filled sites. Adsorption and desorption hysteresis is another phenomenon that has been studied experimentally for sorption media that have been exposed to multiple adsorption/desorption cycles (Cox et al., 1997, Piwowarczyk et al., 2011, Singh *et al*., 2008, Wang, 2013). Green sorption media which minimize adsorption and desorption hysteresis provide an efficient and cost-effective option.

2.1.2. *Chapter Objectives*

The objective of this chapter is to establish the adsorptive and desorptive characteristics of the media mixture and its individual components under equilibrium and dynamic conditions. Equilibrium testing is done through batch tests of adsorption and desorption in order to establish the adsorption and desorption isotherms and to provide screening of potential desorbing agents. Batch tests are further conducted over multiple adsorption-desorption cycles to quantify the hysteresis and change in adsorption capacity over multiple adsorption/desorption cycles. In addition, kinetic studies are conducted for both adsorption and desorption to establish the kinetic reaction order and rate coefficients of the

15

sorbent/sorbate and sorbent/desorbate systems. The culmination of this work is in a dynamic adsorption evaluation through conducting a column breakthrough study on the media mixture and individual components. The column breakthrough study provides a simulation of a field application and provides key engineering design variables such as adsorption capacity and life expectancy.

2.2. <u>Methodology</u>

2.2.1. *Batch Adsorption Tests*

Batch adsorption tests were conducted using 300 mL distilled water spiked with Fisher Scientific 1000 ppm copper standard (copper nitrate). Varying copper solution concentrations of 0.2, 0.6, 1.0, 2.0, and 3.0 mg$\cdot$L^{-1} were added to 500 mL flasks containing 50g of expanded clay and tire chunk, 30 g of media mixture, and 10 g of coconut coir. To discern the effect of the contact time on copper adsorption, batch adsorption tests were conducted within the range that would be experienced in a field application by exposing the media to copper solution for 30 and 60 minutes with a pH of 3.85. In addition, batch adsorption tests at a 60-minute contact time were conducted with a pH of 5.6, representing typical conditions during acid rain, and a pH of 7.0, which represents typical conditions for stormwater runoff. During all tests, the flasks were mixed thoroughly on on a New Brunswick Scientific *Excella E2* shaking platform at 200 rpm and were covered with Parafilm to avoid external disturbances After mixing, the solution was extracted from the flasks, filtered through a 0.45 µm filter, and analyzed in triplicate using the United States Environmental Protection Agency (USEPA) Bicinchoninate method no. 8506 and a HACH DR 2800 spectrophotometer. In all tests, the temperature was kept at 23°C± 3.0 °C and the pH was adjusted using NaOH and HCl$_{(aq)}$.

2.2.2. *Screening of Desorbing Agents and Batch Desorption Tests*

Desorption tests with 4 different desorbing agents were carried out on the copper-loaded media which had been in contact with adsorbate solution for 60 minutes. The selected desorbing agents were DI water, 0.1M HCl, 0.1M HNO_3, and 0.1M H_2SO_4. For each desorbing agent, duplicates of 5 g media mixture, tire chunk, and expanded clay, and 1 g of the coconut coir were exposed to 30 mL of desorbing solution for 180 minutes on a shaking platform at 200 rpm. All media was oven-dried at 75 C for a minimum of 36 hours prior to the test. After mixing, the solution was extracted from the flasks, adjusted to a pH between 4 and 6 using 5.0 N KaOH, filtered through a 0.45 μm filter, and analyzed individually using the USEPA Bicinchoninate method no. 8506.

Relative desorption strength among the 4 desorbing agents was evaluated using the desorption efficiency as the common indicator, defined below:

$$Desorption\ Efficiency = \frac{C_e V}{q_{0D} m} \times 100\% \tag{1}$$

where q_{0D} is the solid-phase copper concentration (mg·g^{-1}) before desorption, m is the mass of media (g), C_e (mg·L^{-1}) is the liquid-phase copper concentration in the desorbing solution, and V (L) is the volume of desorbing solution.

Batch desorption tests were conducted on media which had been in contact with adsorbate solution for 30 minutes with 300 mL 0.1 M HCl as the desorbing agent. The desorbing agent was added to 500 mL flasks containing 50g of expanded clay and tire chunk, 30 g of media mixture, and 10 g of coconut coir. The flasks were then mixed thoroughly for 30 minutes on a shaking platform at 200 rpm.

2.2.3. *Adsorption and Desorption Equilibria (Isotherms)*

Conducting an equilibrium study of the adsorption media mixture allows characterization of the sorption mechanisms and comparison of the adsorption capacities and affinities of the different types of media mixture for copper in solution. Batch adsorption tests were carried out on the media to establish the equilibrium adsorption isotherms for the media mixture and individual media. The Langmuir and Freundlich equations were the two isotherm models employed for this study, given below in their nonlinear form. To discern the effect of the contact time on copper adsorption, batch adsorption tests were conducted within the range that would be experienced in a field application by exposing the media to copper solution for 30 and 60 minutes.

$$q = K_f C_e^{1/n} \tag{2}$$

$$q = q_{max} \frac{K_L C_e}{1 + K_L C_e} \tag{3}$$

where q is the solid-phase copper concentration (mg·g^{-1}), C_e (mg·L^{-1}) is the liquid-phase copper concentration, K_f (mg·g^{-1}) is the Freundlich adsorption coefficient, n (dimensionless) is the nonlinearity factor, K_L (mg·L^{-1}) is the Langmuir adsorption coefficient, and q_{max} (mg·g^{-1}) for the adsorption isotherm is an measure of the maximum adsorptive capacity of the media for copper.

Batch desorption tests were carried out on the media to establish the equilibrium desorption isotherms for the media mixture and individual media. Data from the batch desorption tests were fit to both the and Langmuir equations for desorption isotherms:

$$q = K_{f,D} C_{e,D}^{1/n} \tag{4}$$

$$q = q_{max,D} \frac{K_{L,D} C_{e,D}}{1 + K_{L,D} C_{e,D}} \tag{5}$$

where q is the solid-phase copper concentration (mg·g^{-1}), $C_{e,D,}$ (mg·L^{-}1)is the copper concentration in the desorbing solution, $K_{f,D}$ (mg·g^{-1}) is the Freundlich desorption coefficient, n (dimensionless) is the nonlinearity factor, $K_{L,D}$ (mg·L^{-1}) is the Langmuir desorption coefficient, and $q_{max,D}$ (mg·g^{-1}) for the desorption isotherm an indicator of the desorption capacity of the sorbent-desorbate system. The Freundlich and Langmuir isotherm parameters for adsorption and desorption were optimized by minimizing root mean squared error (RMSE) between the experimental data and the predicted isotherm equation.

2.2.4. *Adsorption and Desorption Kinetics*

The kinetics of the adsorption reaction were observed experimentally and fit to both the classical rate law kinetic equations and the Lagergren kinetic equations for adsorption. The rate law kinetic equations were adapted for adsorption reactions by assuming that the liquid-phase copper concentration, C is related to the initial liquid-phase copper concentration, C_0, by a reaction rate coefficient, k. The data was fit to both first and second-order kinetic equations by minimizing the root mean square error (RMSE) between the kinetic adsorption data and models. For first-order kinetics, the kinetic equation takes the form:

$$C = C_0 e^{-k_1 t} \tag{6}$$

where k_1 (min^{-1}) is the reaction rate constant. For second-order kinetics, the kinetic equation takes the form:

$$\frac{1}{C_e} = \frac{1}{C_0} + k_2 t \tag{7}$$

where the reaction rate constant, k_2 is in units of L·mg^{-1}·min^{-1}.

19

The Lagergren pseudo-first and pseudo-second order kinetic equations are given as:

$$q = q_0(1 - e^{-k_{P1}t}) \qquad (8)$$

$$\frac{t}{q} = \frac{1}{q_0 k_{P2}{}^2} + \left(\frac{1}{q0}\right)t \qquad (9)$$

where q_0 (mg·g^{-1}) is the amount of adsorbed copper at adsorption equilibrium, q (mg·g^{-1}) is the amount of copper that has been adsorbed, k_{P1} is the reaction rate constant (min^{-1}) for the pseudo-first order adsorption reaction, and k_{P2} is the reaction rate constant (g·mg^{-1}·min^{-1}) for the pseudo-second order adsorption reaction. Adsorption kinetic data was obtained by exposing 500 mL flasks containing 50g of expanded clay and tire chunk, 30 g of media mixture, and 10 g of coconut coir to 300 mL of 3.0 mg·L^{-1} Cu solution for 1 hour on a shaking platform at 200 rpm. Samples were taken at predetermined times and analyzed using the methods presented in Section 2.2.1.

Desorption kinetic data was obtained by exposing 500 mL flasks containing 50g of expanded clay and tire chunk, 30 g of media mixture, and 10 g of coconut coir, which had been exposed to 3.0 mg·L^{-1} Cu for 30 minutes, to 300 mL of 0.1 M HCl. Samples were taken at predetermined times and analyzed using the methods presented in Section 2.2.2. The kinetic desorption data was fit to both the classical chemical reaction kinetic equations and the Lagergren kinetic equations for sorption. The rate law kinetic equations were adapted for desorption reactions by assuming that the remaining sorbed copper concentration, $q(t)$ is related to the initial sorbed copper concentration, q_0, by a reaction rate coefficient, k. The data was fit to both first and second-order kinetic equations by minimizing the sum of the squared error between the kinetic desorption data and the model. For first-order kinetics, the kinetic equation takes the form:

$$q = q_0 e^{-k_{1D}t} \qquad (10)$$

where k_{1D} (min^{-1}) is the reaction rate constant. For second-order kinetics, the kinetic equation takes the form:

$$\frac{1}{q} = \frac{1}{q_0} + k_{2D}t \tag{11}$$

where the reaction rate constant, k_{2D} is in units of g·mg^{-1}·min^{-1}.

The Lagergren pseudo-first and pseudo-second order kinetic equations can be adapted for desorption by assuming that the rate of desorption is proportional to the number of metal-filled sites and the square of the number of metal-filled sites, respectively (Njikam and Schiewer, 2012). The pseudo-first order kinetic equation is given as:

$$q_D = q_{0D}(1 - e^{-k_{P1D}t}) \tag{12}$$

where q_{0D} (mg·g^{-1}) is the amount of desorbed copper at desorption equilibrium, q_D (mg·g^{-1}) is the amount of copper that has been desorbed, and k_{P1D} is the reaction rate constant (min^{-1}) for the pseudo-first order desorption reaction. The pseudo-second order kinetic equation is given as:

$$\frac{t}{q_D} = \frac{1}{q_{0D}k_{P2D}^2} + \left(\frac{1}{q_{0D}}\right)t \tag{13}$$

where k_{P2D} is the reaction rate constant (g·mg^{-1}·min^{-1}) for the pseudo-second order desorption reaction.

2.2.5. *Cyclic Adsorption and Desorption*

Re-use of sorption media through multiple sorption-desorption cycles inevitably results a decrease in performance each cycle in terms of total metal ions removed. A reduction in the number of available sorption sites occurs due to incomplete desorption of cations undergoing reversible sorption

reactions and the occurrence of non-reversible sorption reactions. Adsorption/desorption cycles were simulated by conducting batch experiments using the methods presented in Sections 2.2.1 and 2.2.2. For each media type, 5 flasks filled with a constant mass of adsorbent (50 g expanded clay and tire chunk, 30 g mixture, 10 g coconut coir) were exposed to 300 mL varying copper solution concentrations of 0.2, 0.6, 1.0, 2.0, and 3.0 mg·L^{-1} for 30 minutes. The media was then rinsed with about 300 mL of DI water and exposed to 300 mL of 0.1M HCl for 30 minutes. After desorption batch tests, the media were rinsed again with about 300 mL of DI water. This process was done for 3 adsorption/desorption cycles. The change in adsorption performance between successive cycles may also be quantified by the ratio $K_{f,i+1}/K_{f,i}$, where i represents the number of adsorption/desorption cycles the media has gone through. In this case, a ratio of 1 implies no decrease in adsorption, while a ratio less than 1 implies a decrease in adsorption.

2.2.6. *Dynamic Adsorption (Column Breakthrough) Study*

A laboratory column test is a physical model that provides a simulation of field conditions, given a controlled set of experimental conditions (Hossain et al., 2010). For the sorption media mixture, a column test simulates the potential field application of the sorption media in a baffle box with a constant flow rate provided by a pump. The test was set-up as an upward-flow system with three Plexiglas columns with a diameter of 5.1 cm and a length of 30.5 cm (Figure 2.1). The columns each contained a uniform mass of sorption media, which was oven-dried at 75 C for a minimum of 36 hours to eliminate possible biotic activity so that only physiochemical reactions occur in the experiments. 36 hours was determined as the time required to reach a constant mass under drying conditions of 75 C for the whole range of media. In addition to the sorption media, glass beads and filter fabric were provided at the bottom of the columns to assist in dispersion, and filter fabric was provided at the top of the columns to

prevent outward flow of fine particles. The three columns were exposed to identical influent conditions

and flow rates, to provide triplicate measurements for each test.
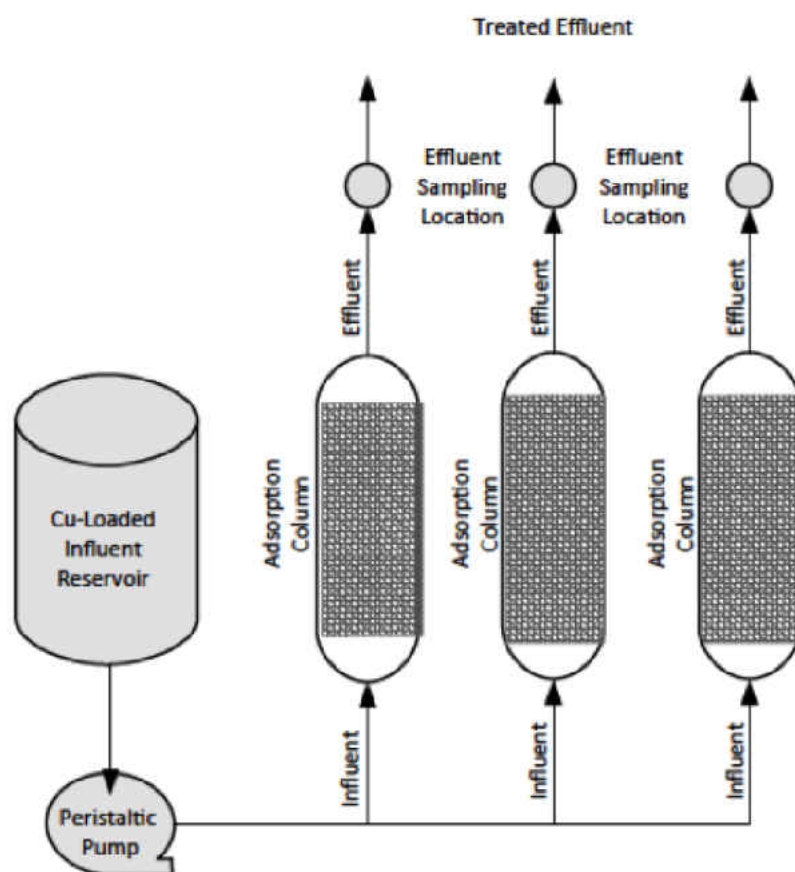
Figure 2.1 Schematic diagram of the column test.

To examine how the adsorption capacity varied among the individual components of the media

under dynamic conditions, a series of column tests were run with identical influent conditions and HRT,

which was calculated as the empty-bed contact time. The influent conditions were 1 mg·L^{-1} Cu in distilled

water and a 30 minute HRT was designated. Influent concentrations of the adsorbent were prepared by

spiking single-distilled water with copper standard solution. Distilled water was used as the liquid matrix in order to ensure only sorbate-sorbent reactions were occurring. To account for varying adsorption characteristics and BTCs among the media types, two different dynamic adsorption models were employed to develop breakthrough curves (BTCs) for the column test data. The Bohart-Adams Model, a classical BTC model that has been successfully used on numerous column studies for heavy metal sorption, and the Modified Dose-Response Model, a more general, empirically-based model.

The Bohart-Adams (B-A) is one of the most commonly used dynamic adsorption models and has shown good correlation to data from column studies of heavy metal sorption. The model assumes pseudo-first-order reversible reaction kinetics and a symmetrical breakthrough curve. For the case of a single reactant, the pseudo-first-order reaction kinetics can be simplified to first-order reaction kinetics, which is verified by the kinetics study for the media mixture and individual media components. From the model, the maximum equilibrium media uptake can be predicted, from which life expectancy of the media can be estimated. The original form, first presented by Bohart and Adams (1920) is given as:

$$\frac{C}{C_0} = \frac{exp(bC_0\left(t-\frac{L}{v}\right))}{exp\left(bC_0\left(t-\frac{L}{v}\right)\right)+exp\left(\frac{bq_0L}{v}\left(\frac{1-\varepsilon}{\varepsilon}\right)\right)+1} \tag{14}$$

By assuming that t >> L/v and disregarding the "1" term in the denominator (Chu, 2010), the model takes the form:

$$\frac{C_e}{C_0} = \frac{1}{1+exp(K_{BA}(a\frac{L}{u}-C_0\,t))} \tag{15}$$

where C_e (mg·mL^{-1}) is the effluent concentration, C_o (mg·mL^{-1}) is the influent concentration, K_{BA} (mL·mg^{-1}min^{-1}) is the rate constant in the B-A model, a is the equilibrium media uptake per unit bed

volume, L is the length of the media bed, and u is the Darcy velocity of the fluid through the media bed.

This can be further simplified to easily measurable variables by multiplying the exponential term by Q/Q,

where Q is the flow rate (mL·min^{-1}):

$$\left(a\frac{L}{u} - C_0 t\right)\frac{Q}{Q} = s\;\frac{a\frac{L}{u}Q - C_0 tQ}{Q} = \frac{m_{adsorbate} - C_0 V}{Q} = \frac{q_0 m - C_0 V}{Q} \tag{16}$$

where, q_o (mg adsorbate·g^{-1} media) is the equilibrium media uptake when C_e/C_o reaches an asymptotic

value, m (g) is the total media mass in the column, and V (mL) is the throughput volume. The model then

takes the simplified form:

$$\frac{C_e}{C_0} = \frac{1}{1 + exp(K_{BA}\left(\frac{q_0 m - C_0 V}{Q}\right))} \tag{17}$$

The model is presented in its linear form, as given by Chu. (2010),

$$ln\left(\frac{C_0}{C_e} - 1\right) = \frac{K_{BA}q_0 m}{Q} - K_{BA}C_0 t \tag{18}$$

From experimental design and measurements in the column test, the input parameters m, Q, t, C_e,

and C_o are known quantities. Thus, the B-A model rate constant, K_{BA}, and q_0 are derived by plotting

$ln[(C_e/C_0) -1]$ vs. t and using linear regression to estimate the model parameters.

For breakthrough curves of sorption media that exhibit asymmetrical behavior, the modified

dose-response (MDR) model can be applied. Yan et al. (2001) found that this model minimizes the error

presented by the Thomas model at the lower and higher time periods of the breakthrough curve. As it is

an empirically derived model, no specific reaction kinetics are assumed. Like the B-A model, the

maximum equilibrium media uptake can be determined from the MDR model, from which the life

expectancy of the media can be estimated. The linear and non-linear forms are presented below,

respectively:

$$ln\left(\frac{C_e}{C_0-C_e}\right) = a_{mdr}\,ln(C_0Qt) - a_{mdr}ln(q_0m) \tag{19}$$

$$\frac{C_e}{C_0} = 1 - \frac{1}{1+(\frac{C_0Qt}{q_0m})^{a_{mdr}}} \tag{20}$$

where a_{mdr} (mL·mg^{-1}min^{-1}) is the is the modified dose-response model constant. Like with the B-A model, the input parameters m, Q, t, C_e, and C_o are known quantities, and the model parameters a_{mdr} and q_0 are obtained by conducting linear regression with the linear form of the model.

To determine whether there is a significant difference between the resulting BTCs generated using the different media, a two-tailed t-test on a normal regression analysis was used to compare the individual column tests. The raw data from each column test were first linearized by plotting $ln[(C_o/C_e) - 1]$ vs. t (time). Then, they were fit to the linear regression model in equation (22) which was used to compare the differences in the adsorption curves generated by the different media compositions:

$$\hat{y} = \beta_0 + \beta_1 x_1 + \beta_2 x_2 + \beta_3 x_1 x_2 \tag{21}$$

where $\hat{y}$ is the predicted $ln(C_o/C_e-1)$, x_1 is time (minutes), and x_2 is an indicator variable. To determine the difference between the use of the media mixture and the tire chunk, for example, the indicator variable, x_2, that takes on the value 1 when the media type is mixture and takes on the value 0 if the media type is tire chunk. Consequently, the linear model used for prediction is $\hat{y} = \beta_0 + \beta_2 + (\beta_1 + \beta_3)x_1$ when the media type is mixture, and otherwise, the prediction is $\hat{y} = \beta_0 + \beta_1 x_1$ when the media type is tire chunk. The same methodology was used to compare each of the other media combinations, bringing the total number of comparisons to 6.

To compare the intercepts of the linear equations which were developed, the null hypothesis, H$_0$ is that $\beta_2 = 0$ and the alternative hypotheses, H$_1$ is that $\beta_2 \neq 0$. Thus, if the null is rejected, the regression parameters representing the intercepts of the line are significantly different. This follows for the

26

comparison of slopes having a hypotheses of H_o: $\beta_3 = 0$ and H_1 : $\beta_3 \neq 0$. Each analysis was considered statistically significant at a confidence interval of 95% ($\alpha=0.05$). The P-value results from the two-tailed t-test indicate if there is significant difference in the slope and intercept of the copper adsorption curves being compared. Statistical analyses were performed using R statistical software (2013).

2.3. Results and Discussion

2.3.1. Adsorption and Desorption Isotherms

The adsorption data for varying contact times were fit to both the Langmuir and Freundlich models and the correlation coefficients for the equilibrium adsorption data, presented in Table 2.2 and Table 2.3 show that both models fit the sorption pattern well for both contact times, with R^2 values all greater than 0.80. The strong correlation with the Langmuir model suggests that the inherent assumption of monolayer adsorption generally holds true for all media types. Additionally, this points to ion exchange as the dominant adsorption mechanism (Pehlivan et al., 2006).

Table 2.2. Summary of Langmuir isotherm parameters for the 30 and 60 minute contact times.

Media	30 min. Contact Time			60 min. Contact Time		
	K_L (mg·L^1)	q_{max} (mg·g^{-1})	R^2	K_L (mg·L^{-1})	q_{max} (mg·g^{-1})	R^2
Mixture	1.664	0.047	0.96	0.202	0.321	0.98
Tire Chunk	0.078	0.027	0.97	0.120	0.017	0.96
Exp. Clay	0.321	0.068	0.96	4.660	0.019	0.98
Coconut Coir	2.374	0.218	0.89	0.024	20.518	0.93

Table 2.3. Summary of Freundlich isotherm parameters for the 30 and 60 minute contact times.

Media	30 min. Contact Time			60 min. Contact Time		
	K_f (mg·g^{-1})	n	R^2	K_f (mg·g^{-1})	n	R^2
Mixture	0.034	1.42	0.92	0.054	1.11	0.98
Tire Chunk	0.002	0.88	0.94	0.002	1.35	0.95
Exp. Clay	0.017	1.08	0.93	0.019	1.91	0.92
Coconut Coir	0.246	1.31	0.80	12.0	0.41	0.96

A deepened comparison of the model parameters across the media mixture and its components is shows that the coconut coir exhibits the highest affinity for copper (q_{max} = 0.218 and 20.518 mg·g^{-1}), followed by media mixture, expanded clay, and tire chunk. For the mixture and coconut coir, the adsorption of copper increased with a higher contact time significantly, however the expanded clay and tire chunk showed a small decrease in adsorption capacity. The values of the Freundlich nonlinearity parameter, n, indicate that almost all isotherms are convex in nature, with values greater than 1. However, the isotherm for coconut coir at the 60 minute contact time is highly concave ($n \ll 1$), suggesting that all types of adsorbate have equal affinity for the adsorbent, under these conditions. (Saywer et al., 2003).
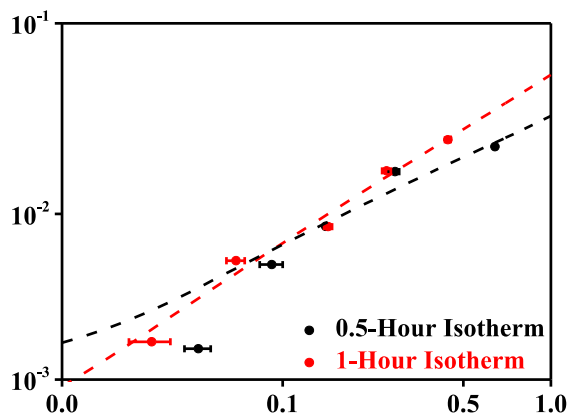
y=0.2462x$^{0.798}$
(R^2=0.802)

Figure 2.2- Freundlich isotherms for (a) media mixture (b) tire chunk (c) expanded clay and (d) coconut coir. The error bars represent the standard deviation of the triplicate liquid-phase copper concentration measurements.

The equilibrium test results for varying pH identify that the adsorption of copper to the media mixture and its individual components is a pH dependent phenomenon. In general, an increase in the pH led to a higher adsorption of copper, with the peak sorption capacity being realized at a pH of 7.0 for the tire chunk, expanded clay, and coconut coir. The equilibrium sorption capacity for coconut coir ($q_{max}=$ 71.1 mg·g^{-1}) at a typical stormwater pH of 7 compares well to other published studies of green sorption media (Table 2.1). This increase in sorption may be attributed to fewer hydrogen ions in solution that may compete with the copper for adsorption to negatively-charged surfaces. This suggests that the inherent

29

conditions of stormwater runoff provide an environment most conducive to copper sorption on the media, within the studied pH range.

The media mixture exhibited the highest adsorption at a pH of 5.6 (q_{max} = 0.502 mg·g^{-1}), with a mild decrease from a pH 5.6 to 7.0, although the effect of pH on it was milder compared to that of the individual media components. This could suggest the presence of an interaction effect, where protons released during ion exchange with the weaker adsorbents, expanded clay and tire chunk, may preferentially bond to the stronger adsorbent, coconut coir, making the overall change in adsorption appear milder that that for the individual media components. For the tire chunk and expanded clay at a pH of 7, the liquid-phase Cu concentration after adsorption was nearly identical for initial Cu concentrations of 2.0 and 3.0 mg·L^{-1}, which showed deviation from the observed adsorption pattern at lower initial concentrations (Figure 2.3). Fitting this data to the Langmuir model led to steeper isotherms which may have over-estimated the equilibrium adsorption capacity, q_{max}, due to this anomaly.

Table 2.4. Summary of isotherm parameters for the media mixture, tire chunk, expanded clay, and coconut coir at three pH levels.

Media	Langmuir Isotherm			Freundlich Isotherm		
	K_L (mg·g^{-1})	q_{max}	R^2	K_f (mg·g^{-1})	n	R^2
pH = 3.85						
Mixture	0.202	0.321	0.98	0.054	1.11	0.98
Tire Chunk	0.120	0.017	0.96	0.002	1.35	0.95
Exp. Clay	4.66	0.019	0.98	0.019	1.91	0.92
Coconut Coir	0.024	20.6	0.93	12.0	0.41	0.96
pH = 5.6						
Mixture	0.200	0.502	0.98	0.072	1.33	0.99
Tire Chunk	2.20	0.006	0.99	0.004	2.38	0.93
Exp. Clay	1.09	0.021	0.96	0.011	1.47	0.95
Coconut Coir	0.020	43.9	0.91	10.7	0.449	0.96
pH = 7.0						
Mixture	0.200	0.395	0.97	0.061	1.254	0.98
Tire Chunk	0.031	0.497	0.81	0.016	0.933	0.81
Exp. Clay	0.015	5.97	0.91	2.35	0.402	0.94
Coconut Coir	0.017	71.1	0.99	8.85	0.548	0.99
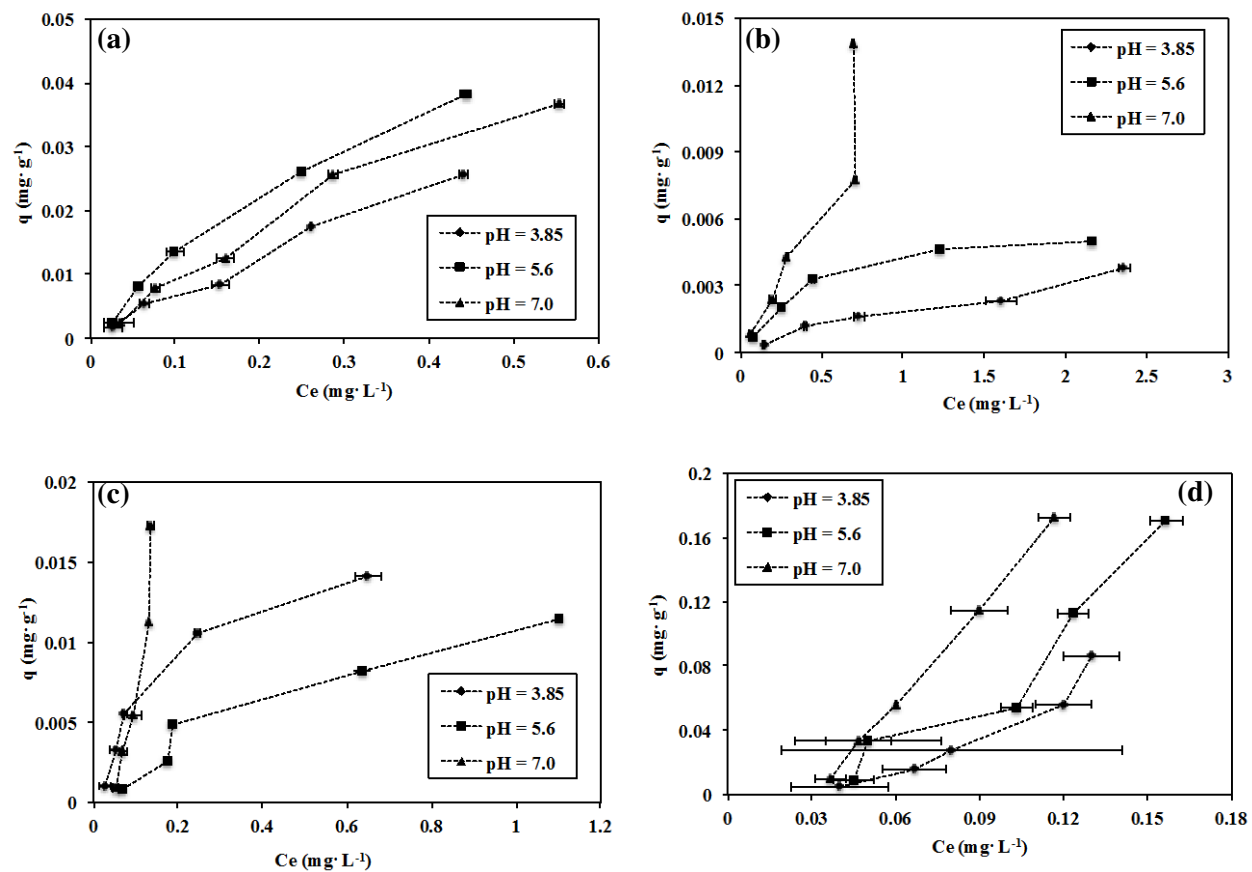
Figure 2.3. Isotherms for (a) media mixture (b) tire chunk (c) expanded clay and (d) coconut coir at 3 different pH levels. The error bars represent the standard deviation of the triplicate liquid-phase copper concentration measurements.

The results presented in Figure 2.4 show that regeneration of the media is quite successful with the use of strong acids. This is particularly true for hydrochloric acid, which provided 83%, 84%, and 48% desorption efficiencies for the expanded clay, coconut coir, and media mixture, respectively. The tire chunk exhibited a desorption efficiency of over 100% for HCl, which can be pointed to leaching of pre-existing copper content in the tire material from copper-containing brake dust and the tire manufacturing process. The success of strong acids as a desorbing agent points to ion exchange as being the dominant sorption mechanism, as the adsorption isotherm modeling suggested. On the other hand, desorption under DI water was nearly negligible, which suggest only a small contribution from physical sorption toward the overall copper adsorption.
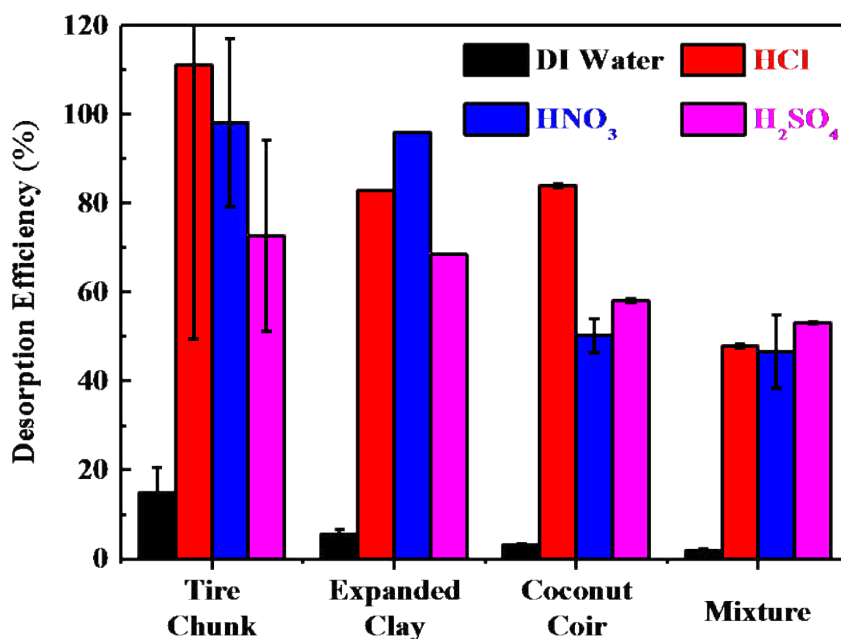
Figure 2.4 Desorption efficiencies for each media type using DI water, 0.1 M hydrochloric acid, 0.1 M nitric acid, and 0.1 M sulfuric acid as desorbing agents.

Data from batch desorption tests were fit to both the Langmuir and Freundlich isotherm equations, and they fit both isotherms reasonably well. However, the Freundlich equation resulted in a better prediction for all media types, particularly for the expanded clay, as shown in Table 2.5. The Freundlich parameter K_f, which is also the slope of the desorption isotherm indicates the relative strength, or effectiveness of the desorption process on the Cu-loaded media. The values for K_f, as indicate that the coconut coir, followed by the expanded clay and the media mixture experienced the strongest desorption, which is consistent with Figure 2.4. It is worth noting that all of the Freundlich nonlinearity parameters (n) are significantly less than 1, which correspond to concave-type isotherms. This is in contrast to the convex-type isotherms typically observed for adsorption data (Febrianto et al., 2009) and those that were observed for the Freundlich adsorption isotherms of the media. This suggests that desorption efficiency decreases as the amount of initial sorbed copper increases, resulting in a highly nonlinear, concave isotherm.

For all media types, a desorption efficiency greater than 100% was observed for the media that had been exposed to sorbate of the lowest concentration (0.2 mg·L^{-1}). As a result, a shift factor was applied to the desorption data to provide positive values of q for model fitting. While this was mathematically necessary, it did introduce a small amount of error in the modeling effort. The modeling results for the tire chunk are not shown, as the existing copper content in the material skewed the results, resulting in apparent desorption efficiencies over 100% over the entire range of initial sorbate concentrations.

Table 2.5. Summary of desorption isotherm parameters

Media	Langmuir Isotherm			Freundlich Isotherm		
	$K_{L,D}$ (mg·L^{-1})	$q_{max,D}$ (mg·g^{-1})	RMSE (mg·g^{-1})	$K_{f,D}$ (mg·g^{-1})	n	RMSE (mg·g^{-1})
Mixture	0.00217	6.04	0.00207	0.0139	0.741	0.00173
Exp. Clay	-0.293	-0.041	0.00128	0.0730	0.389	0.000216
Coconut Coir	0.00478	15.929	0.00778	0.0791	0.769	0.00603
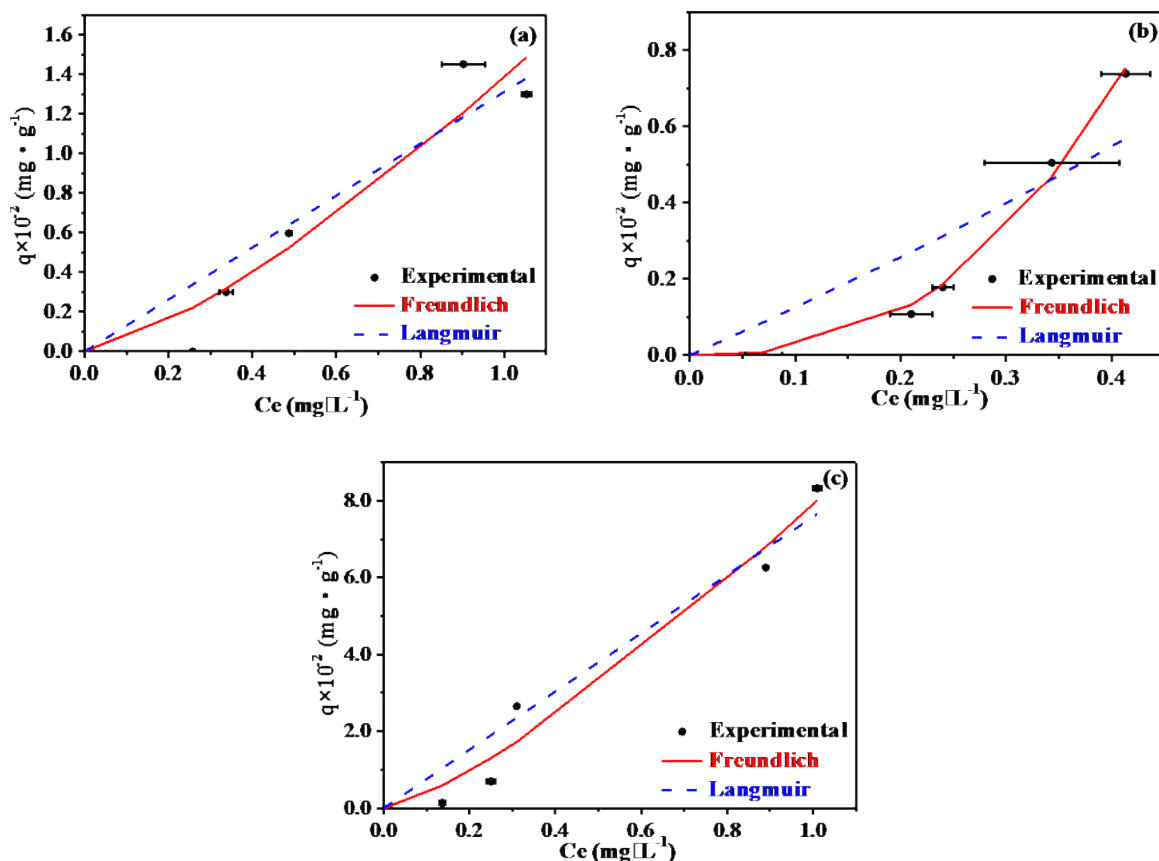
Figure 2.5. Langmuir and Freundlich desorption isotherms for (a) media mixture, (b) expanded clay, and (c) coconut coir

2.3.2. *Adsorption and Desorption Kinetics*

The kinetic data revealed that the adsorption reaction was a relatively fast one, as equilibrium was reached within 60 minutes for all media types, and equilibrium was reached within just 30 minutes for the coconut coir and tire chunk. The kinetic data showed good correlation with both types of kinetic models, as the data was better aligned with the pseudo first- and second-order kinetic models for the media mixture and coconut coir and with the second-order rate law kinetic model for the expanded clay (Table

34

2.6 and Table 2.7). However, while the rate law kinetic models had good correlation over the whole observed time period, there was significant deviation in the later-time data, as seen in Figure 2.7. This can be attributed to the mathematical structure of the rate law equations, as they predict the remaining liquid-phase metal goes to zero as t goes to infinity. For reactions that are adsorbent-limited, the remaining sorbed metal, q_0 actually approaches an asymptotic value at equilibrium. For the Lagergren first- and second-order kinetic equations, however, q approaches q_0 as t goes to infinity, which was assumed to be the observed value of q at t = 60 minutes. As a result, strong correlation was observed with kinetic data for both pseudo first- and second-order reaction models, with R^2 values all above 0.95. The exception was the tire chunk, which exhibited little adsorption for the first 5 minutes, followed by a typical adsorption pattern over the following 15 minutes (Figure 2.7b)).

Table 2.6. Summary of Rate Law kinetic model parameters for adsorption

	First-Order		Second-Order	
Media	K_1 (min^{-1})	R^2	K_2 (g·mL^{-1}·min^{-1})	R^2
Mixture	0.241	0.946	0.114	0.968
Tire Chunk	0.0148	0.929	0.00660	0.944
Exp. Clay	0.115	0.969	0.0626	0.980
Coconut Coir	0.527	0.964	0.300	0.987

Table 2.7. Summary of Lagergren kinetic model parameters for adsorption

	Lagergren Pseudo-First Order			Lagergren Pseudo-Second Order		
Media	K_{P1} (min^{-1})	q_0 (mg·g^{-1})	R^2	K_{P2} (g·mg^{-1}·min^{-1})	q_0 (mg·g^{-1})	R^2
Mixture	0.394	0.0226	0.966	29.2	0.0226	0.985
Tire Chunk	0.0492	0.00675	0.949	10.9	0.00675	0.908
Exp. Clay	0.186	0.0137	0.957	23.1	0.0137	0.957
Coconut Coir	0.828	0.0750	0.982	21.1	0.0750	0.997
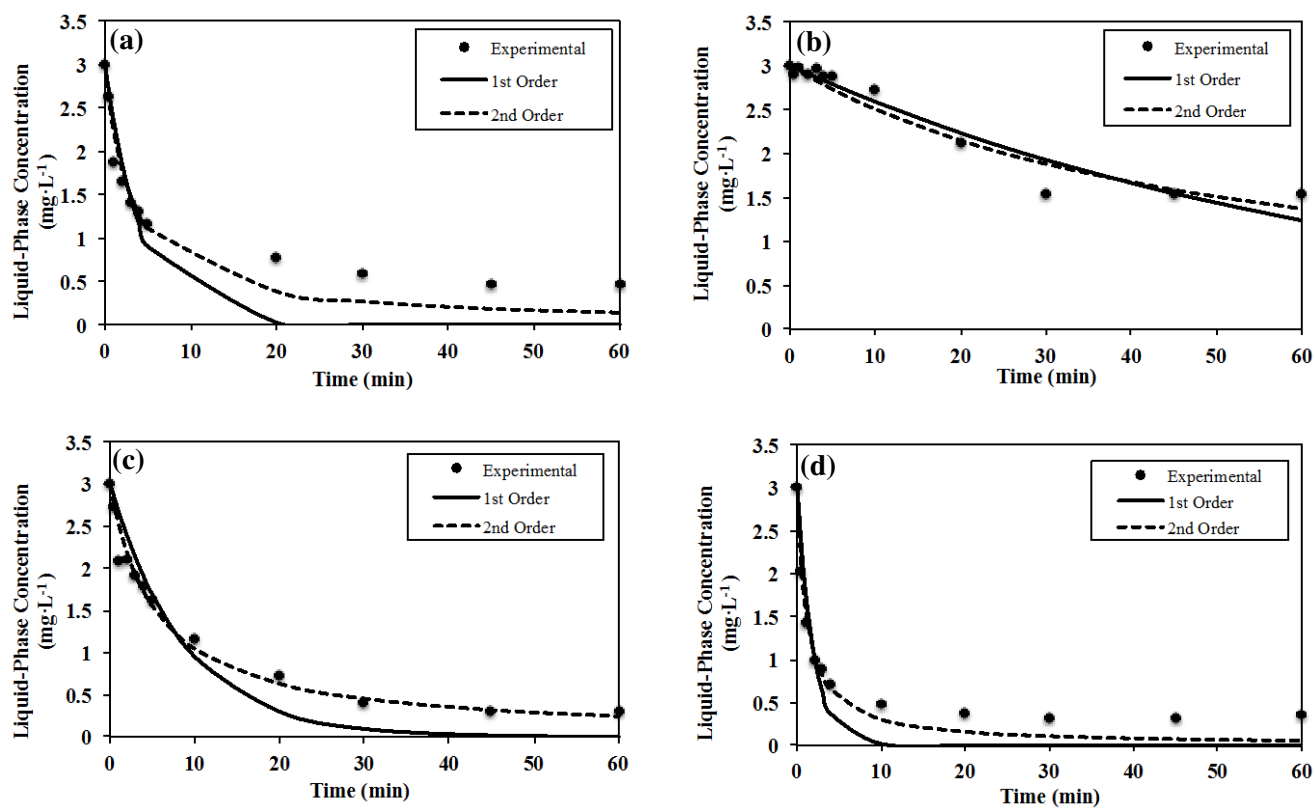
Figure 2.6. Rate Law adsorption kinetics for (a) media mixture (b) tire chunk (c) expanded clay aggregate and (d) coconut coir
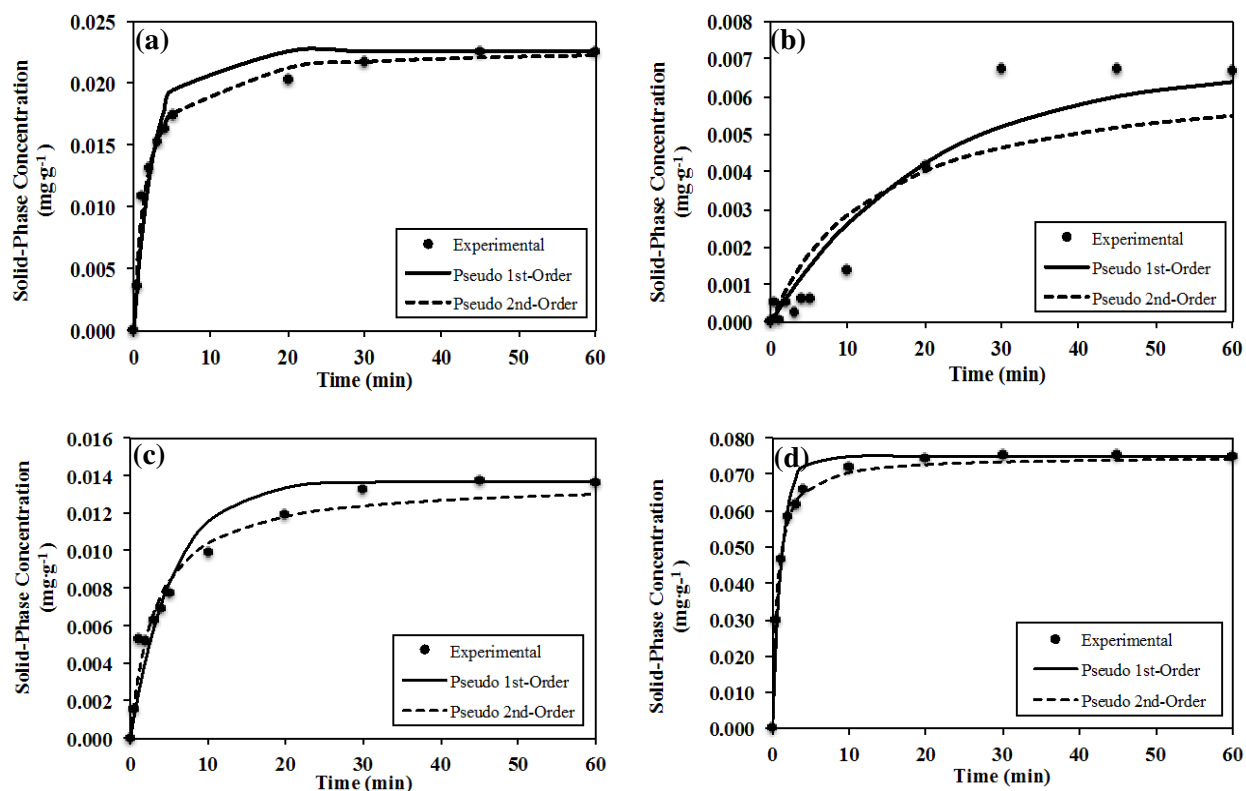
Figure 2.7. Lagergren adsorption kinetics for (a) media mixture (b) tire chunk (c) expanded clay aggregate and (d) coconut coir

The kinetic desorption data revealed that the desorption reaction was a very fast one, with over 50% of desorption occurring within the first 30 seconds for all media types. Equilibrium was reached within 30 minutes, with the exception of the tire chunk. For the rate law kinetic equations, a decrease in correlation was observed as the desorption efficiency decreased (Table 2.8). This can be attributed to the mathematical structure, as it predicts the remaining sorbed metal goes to zero as t goes to infinity. With less than 100% desorption, the remaining sorbed metal, q_{0D} actually approaches an asymptotic value. For the Lagergren pseudo first- and second-order kinetic equations, however, q_{0D} was assumed to be a model parameter, the amount of desorbed copper (mg·g⁻¹) at equilibrium, instead of a variable, the total amount of initial sorbed copper (mg·g⁻¹). As a result of this assumption, strong correlation was observed with

37

kinetic data for both pseudo first- and second-order reaction models, with R^2 values all above 0.96. The exception was the tire chunk, which exhibited typical kinetic characteristics for the 1st 10 minutes, with a slower reaction occurring after that (Figure 2.8). This is most likely attributed to desorption of the sorbed copper within the first 10 minutes, followed by the slow release of the pre-existing copper content in the tire chunk.

Table 2.8. Summary of rate law kinetic model parameters for desorption. Note the tire chunk parameters are not included, since observed desorption was greater than 100% due to pre-existing copper content.

Media	q_0 (mg·g^{-1})	q_{0D} (mg·g^{-1})	Desorption Efficiency (%)	R^2 (1st Order)	R^2 (2nd Order)
Mixture	0.0234	0.0204	87.2	0.894	0.948
Exp. Clay	0.0126	0.0109	86.5	0.917	0.934
Coconut Coir	0.0814	0.0535	65.7	0.657	0.689

Table 2.9. Summary of Lagergren kinetic model parameters for desorption

Media	Lagergren Pseudo-First Order			Lagergren Pseudo-Second Order		
	K_{P1D} (min^{-1})	q_{0D} (mg·g^{-1})	R^2	K_{P2D} (min^{-1})	q_{0D} (mg·g^{-1})	R^2
Mixture	1.39	0.0195	0.959	136	0.0204	0.985
Tire Chunk	1.35	0.00370	0.751	651	0.00388	0.849
Exp. Clay	2.49	0.0105	0.977	464	0.0109	0.994
Coconut Coir	2.27	0.0515	0.977	82.5	0.0535	0.989
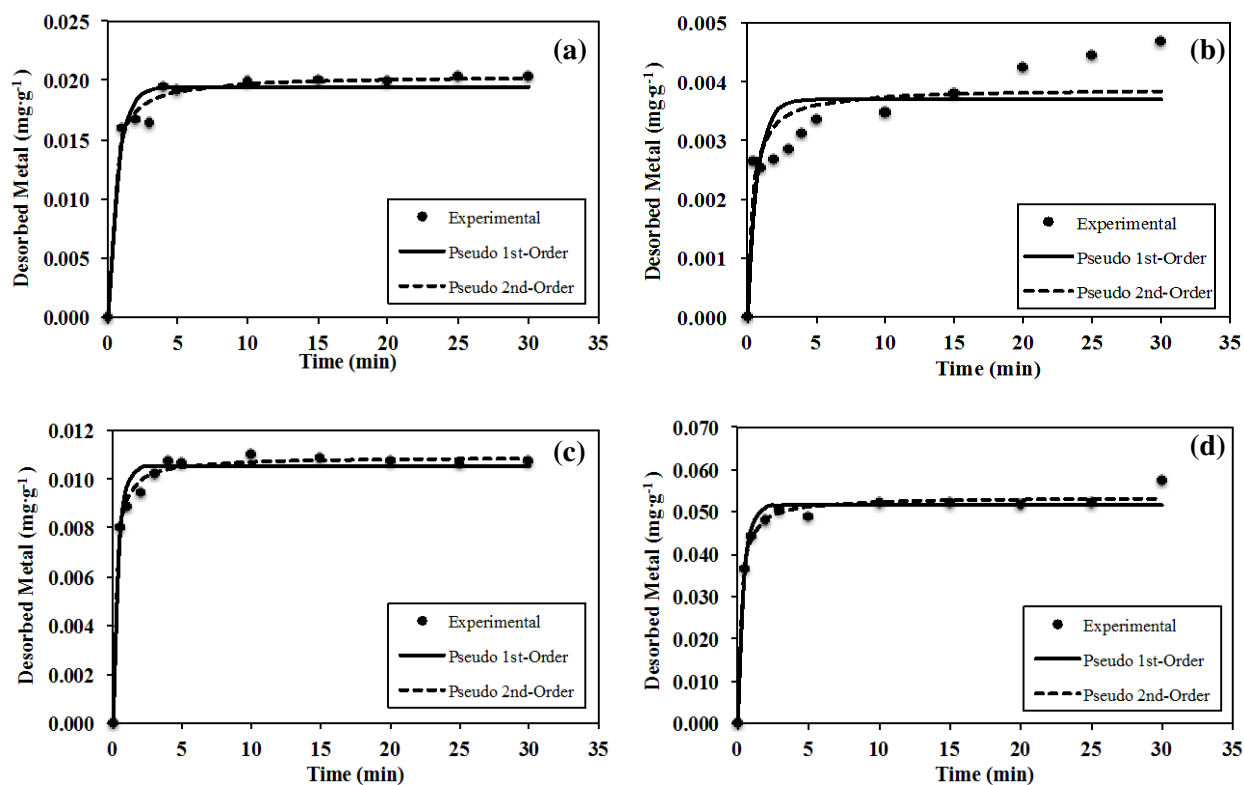
Figure 2.8. Desorption kinetics for (a) media mixture (b) tire chunk (c) expanded clay aggregate and (d) coconut coir.

2.3.3. *Cyclic Adsorption and Desorption*

3 successive adsorption/desorption cycles were carried out on each media type as a batch system with initial copper concentrations ranging from 0.2 to 3.0 mg·L^{-1}. The results showed that the reusability of the media is impacted after just 3 cycles. The sorption of copper on the media decreased by 44%, 100%, 74%, and 19% for the media mixture, tire chunk, expanded clay, and coconut coir, respectively, based on the media with an initial sorbate concentration of 3.0 mg·L^{-1}. Figure 2.9 shows a steep decrease in adsorption for expanded clay between the 1st and 2nd cycles, while the decrease is more gradual for the other media types. This indicates that expanded clay would only serve one useful life cycle if used in isolation. The Freundlich adsorption parameters in Table 2.10 for the successive cycles give further

39

description to the observed decrease in adsorption over multiple cycles. The biggest decrease in

adsorption capacity was observed for the expanded clay between the 1st and 2nd cycles, while the coconut

coir adsorption was the least impacted by the desorption stage.

Table 2.10. Summary of Freundlich adsorption coefficient ratios for 3 adsorption/desorption cycles. Subscripts 1, 2, and 3 refer to the respective adsorption/desorption cycle.

Media	$K_{f,2}/K_{f,1}$	$K_{f,3}/K_{f,2}$
Mixture	0.617	1.045
Exp. Clay	0.222	0.853
Coconut Coir	0.795	0.989
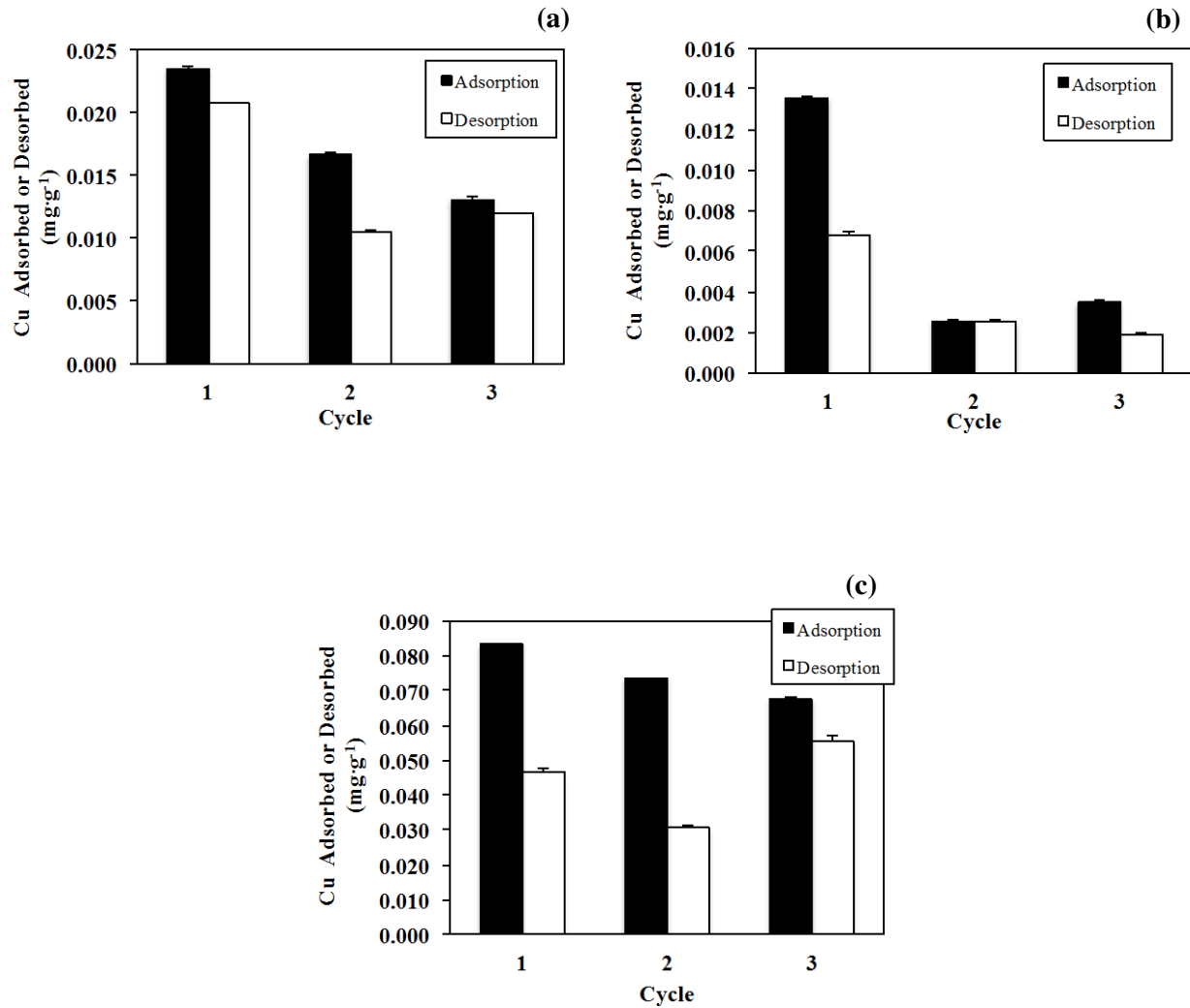
Figure 2.9. Cyclic adsorption/desorption data for (a) media mixture (b) expanded clay aggregate and (c) coconut coir.

2.3.4. *Column Breakthrough Study*

The column adsorption data for the mixture, tire chunk, expanded clay, and coconut coir were fit to both models to evaluate which one best described the adsorption pattern. The results show that the B-A model fits the tire chunk ($R^2 = 0.86$) and expanded clay ($R^2 = 0.97$) well (Table 2.11), while the MDR model best defines the coconut coir ($R^2 = 0.94$) and the media mixture ($R^2 = 0.96$) BTCs (Table 2.12) The

column studies for the mixture and coconut coir were not carried completely to breakthrough ($C_e/C_0 = 1$), as they reached asymptotic rates of removal over time (Figure 2.10). It is hypothesized that either there is a shift in the adsorption rate due to the higher-energy sites being used up in the initial time period, or the adsorptive capacity of the media mixture has been reached and removal is occurring through metal hydroxide precipitation. The latter phenomenon could be caused by an increase in Cu^{2+} concentration within the column due to decreased adsorption and higher pH within the media pore spaces and on the media surface, leading to a lower solubility of $Cu(OH)_2$. Further work would need to be conducted to confirm either of these phenomena. As a result, the linear regression was only carried out over the range of data where the effluent concentration was increasing with time, providing a conservative estimate of actual adsorption capacity.

The discrepancies between the model predictions may be explained by the B-A model assuming symmetrical BTCs (Xu et al., 2013), which the media mixture and the coconut coir clearly do not exhibit (Figure 2.10). Additionally, the presence of precipitation with the inclusion of coconut introduces chemical processes likely not described by the B-A model, while the MDR model is a more generalized sorption model. The similarities between the shapes of the mixture and the coconut coir breakthrough curves suggest that the coconut is the dominant contributor to copper adsorption in the mixed-media matrix.

(a) media mixture
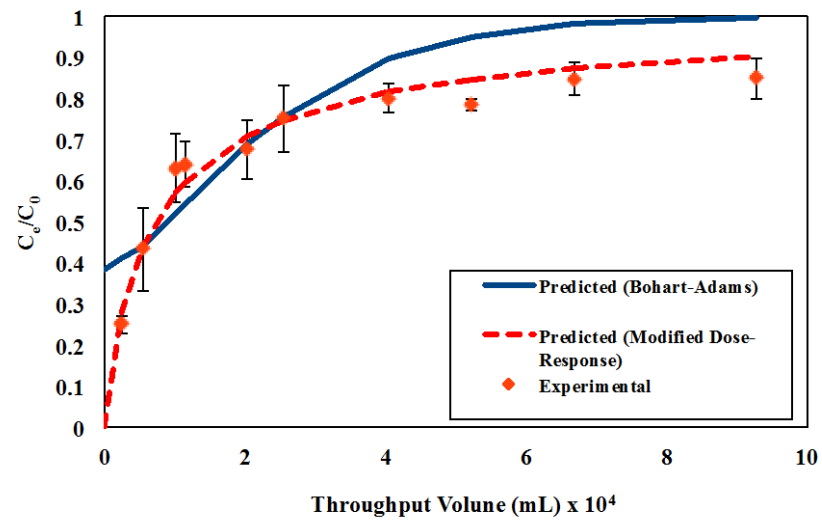
(b) tire chunk
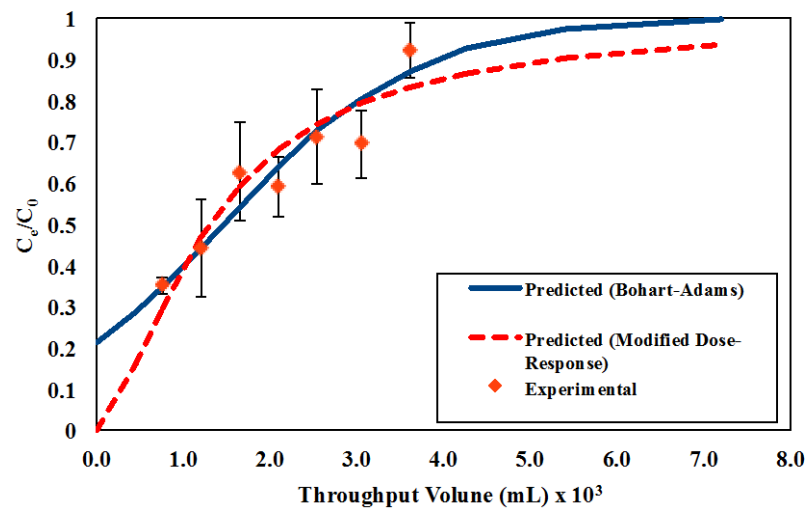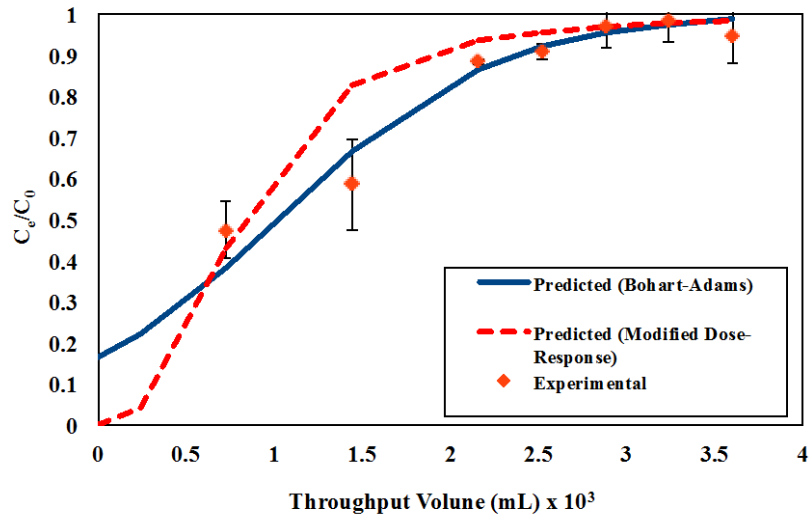
(c) expanded clay

(d) coconut coir
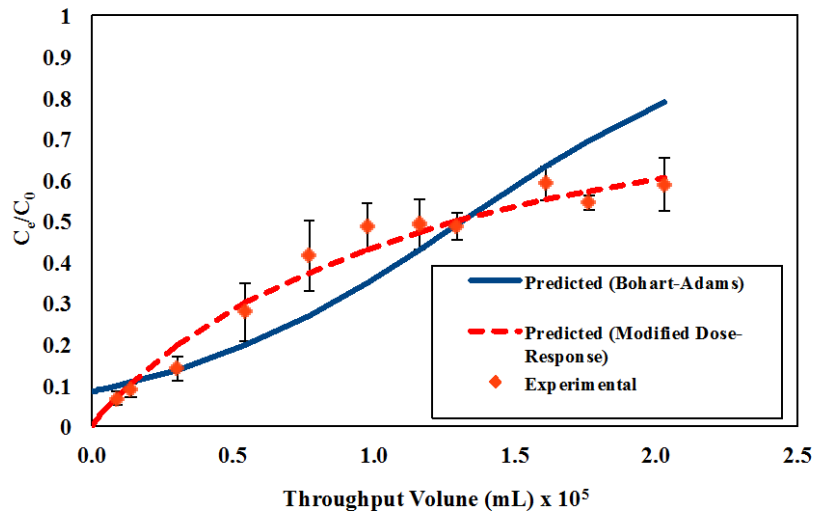
Figure 2.10 Experimental and predicted breakthrough curves for (a) media mixture (b) tire chunk (c) expanded clay and (d) coconut coir. Experimental data points represent an average of the three column measurements and the error bars represent the standard deviation. It should be noted that the horizontal scales have been adjusted for each media type, based on the duration of the column test.

44

The derived model parameter q_0 shows that the coconut coir has a much greater capacity (1.63 mg·g^{-1}) for copper adsorption than the mixture (0.021 mg·g^{-1}), tire chunk (0.0034 mg·g^{-1}) or expanded clay (0.0025 mg·g^{-1}), which is confirmed by the results from the isotherm study. The tire chunk and expanded clay were significantly less effective in isolation than the mixture and reached breakthrough after just 6.25 and 8.25 hours, respectively.

In addition, there exists a discrepancy between the adsorption under equilibrium and under dynamic conditions for the expanded clay. The clay outperformed the tire chunk in the isotherm tests while exhibiting the smallest adsorption capacity during the breakthrough tests. This discrepancy suggests the formation of preferential flow paths, or short-circuiting in the media, decreasing the exposure to possible sorption sites during dynamic conditions.

Table 2.11. Summary of Bohart-Adams (B-A) model parameters obtained from the dynamic adsorption study

Media	BTC Equation[a]	K_{BA} (mL·mg^{-1}·min^{-1})	q_0 (mg·g^{-1})	R^2
Mixture	y = -0.001x + 0.48	0.55	0.025	0.74
Tire Chunk	y = -0.01x + 1.31	8.96	0.0034	0.86
Expanded Clay	y = -0.01x + 1.64	13.00	0.0025	0.97
Coconut Coir	y = -0.0002x + 2.15	0.20	1.46	0.84

[a]Where $y = ln(C_0/C_e - 1)$ and $x = t$ (in minutes)

Table 2.12. Summary of Modified Dose-Response (MDR) model parameters obtained from the dynamic adsorption study

Media	BTC Equation[a]	a_{mdr}	q_0 (mg·g^{-1})	R^2
Mixture	Y = 0.86x – 1.70	0.86	0.021	0.96
Tire Chunk	Y = 1.57x – 0.41	1.57	0.0030	0.78
Expanded Clay	Y = 2.94x + 0.10	2.94	0.0025	0.78
Coconut Coir	Y = 0.97x - 4.72	0.97	1.63	0.94

[a]Where $y = ln(C_e/(C_0-C_e))$ and $x = ln(C_0Qt)$

Establishing statistically significant differences between the column tests is critical in making comparisons and conclusions on media performance. A comparison between the BTCs of each of the

media types was made using a two-tailed t-test based on the linear regression parameters β_2 and β_3 from equation (22). Statistically significant differences were found for all media combinations at the 95% confidence level ($\alpha = 0.05$) for both slope and intercept, with the exception of the tire chunk and expanded clay, which exhibited p values of 0.69 and 0.068 for the slope (β_3) and intercept (β_2), respectively. Physically speaking, this suggests that the media exhibited significantly different characteristics in both initial adsorption and adsorption rate over time, with the exception of the tire chunk compared to the expanded clay, which allows for valid conclusions to be made regarding the adsorptive capacity and efficiency of the different media types based on the column study results.

2.4. <u>References</u>

Acheampong, M.A., Pereira, J., Meulepas, R., and P. Lens. 2011. Biosorption of Cu(II) onto agricultural materials from tropical regions. *J. Chem. Technol. Biotechnol* 86: 1184-1194.

Bohart, G.S., and E.Q. Adams. 1920. Some aspects of the behavior of charcoal with respect to chlorine. *J. Am. Chem Soc* 42: 523–529.

Calisir, F., Roman, F.R., Alamo, L., Perales, O., Arocha, M.A., and S. Akman. 2009. Removal of Cu(II) from aqueous solutions by recycled tire rubber. *Desalinisation*. 249: 515-518.

Cox, L., Koskinen, W., and P.Y. Yen. 1997. Sorption-desorption of imidacloprid and its metabolites on soils. *J. Agric. Food Chem*. 45: 1468-1472.

Febrianto, J., Kosasih, A., Sunarso, J., Ju, Y.H., Indraswati, N., and S. Ismadji. 2009. Equilibrium and kinetic studies in adsorption of heavy metals using biosorbent: A summary of recent studies. *J. Hazard. Mater*. 162: 616-645.

Hossain, F., Chang, N.B., and M. Wanielista. 2010 Modeling kinetics and isotherms of functionalized filter media for nutrient removal from stormwater dry ponds. *Environ Prog Sustainable Energy* 29:, 319-333.

Kyzas, G., Lazaridis, N., and M. Kostoglou. 2014. Adsorption/desorption of a dye by a chitosan derivative: Experiments and phenomenological modeling. *Chemical Engineering J.* 248: 327-336.

Musso, T.B., Parolo, M.E., Pettinari, G., and F.M. Francisca. 2014. Cu(II) and Zn(II) adsorption capacity of three different clay liner materials. *J Environ Management.* 146: 50-58.

Njikam, E., and S. Schiewer. 2012. Optimization and kinetic modeling of cadmium desorption from citrus peels: A process for biosorbent regeneration. *J. Hazard Mater.* 213-214: 242-248.

Pehlivan, E., Cetin, S., and B.H. Yanik. 2006. Equilibrium studies for the sorption of zinc and copper from aqueous solutions using sugar beet pulp and fly ash. *J. Hazard. Mater.* 125: 193-199.

Piwowarczyk, A., and N. Holden. 2011. Adsorption and desorption isotherms of the nonpolar fungicide chlorothalonil in a range of temperate maritime agricultural soils. *Water Air Soil Pollut.* 223: 3975-3985.

Sawyer, C.N., McCarty, P.I., and G.F. Parkin, G.F. 2003. "Water chemistry for environmental engineering and science", 5th ed. New York, McGraw Hill.

Singh, A., Kumar, D., and J.P. Gaur. 2008. Removal of Cu(II) and Pb(II) by *Pithophora oedogonia:* Sorption, desorption, and the repeated use of the biomass. *J. Hazard Mater.* 152: 1011-1019.

Vilar, V., Botelho, C., and R. Boaventura. 2007. Copper desorption from *Geldium* algal biomass. *Water Res.* 41: 1569-1579.

Wang, C., Li, H., Liao, S., Zheng, H., Wang, Z., Pan, B., and B. Xing. 2013. Coadsorption, desorption hysteresis and sorption thermodynamics of sulfamethoxazole and carbamazepine on graphene oxide and graphite. *Carbon* 65: 243-251.

Xu, Z., Cai, J.G., and B.C. Pan 2014. Mathematically modeling fixed-bed sorption in aqueous systems. *J of Zhejiang University – Science A* 14: 155-176.

Yan, G., Virarghavan, T., and M. Chen. A new model for heavy metal removal in a biosorption column. *Ads Sci Technol* 19: 25-43.

CHAPTER 3: MATERIAL CHARACTERIZATION: STRUCTURE AND PROPERTIES

3.1. Introduction

3.1.1. Introduction and Literature Review

As adsorption is a surface reaction, the surface morphology, surface area and internal pore structure of a sorption media govern the amount of adsorption which can take place. Adsorbents which have a rough, irregular surface clearly provide a large amount of surface area for surface sorption. However, an effective adsorbent is one which has a large surface area in its intraparticle surface area, or internal pore network. This pore network is composed of micro- (<2 nm) and mesopores (between 2 and 50 nm, while the macropore network (>50 nm) allows for the bulk movement of fluid through the media (Sing *et al.* 1985). Generally, an inverse relationship has been observed between the internal pore size and the surface area, however if the internal pore sizes are too small, then larger adsorbate molecules may not be able pass through and adsorb to the inner-pore structure (Howe *et al.*, 2012).

A few previous studies have investigated the structural and chemical properties of similar clay, tire rubber, and coconut coir materials as those investigated in this study. Oueslati *et al.* (2009) used X-ray diffraction (XRD) to confirm that, copper sorption occurs through electrostatic attraction and ion exchange in montmorillonite clays, which was confirmed by Musso *et al* (2014) through XRD and Fourier transform infrared spectroscopy (FTIR) on bentonite and calcareous clays. FTIR analysis on coconut coir found that adsorption occurs through a combination of ion exchange with hydroxyl and carboxylic functional groups and electrostatic attraction in coconut coir (Acheampong *et al.*, 2011). Calisir *et al.*, 2009 conducted batch equilibrium experiments for Cu adsorption on tire rubber and found

that adsorption likely occurred through ion exchange with Zn species, although this was not confirmed through any spectroscopy, such as XRD or FTIR.

3.1.2. *Chapter Objectives*

The objectives of the work presented in this chapter are to provide a characterization of the structural and chemical properties of the sorption media mixture and its components at the macro-, meso- and micro-scales, determine the key engineering design variables for a sorption media filter design, and to support the adsorption and desorption testing results in Chapter 2 through imaging and material analysis. Macro-scale physical characterization is done for raw media through a series of ASTM standard tests to describe the porosity, mass-volume relationship, and particle size distribution of the media mixture and its components. Meso- and micro-scale characterization is conducted for media before adsorption, media after adsorption, and media after desorption through FE-SEM imaging, XRD to analyze the crystalline structure, energy dispersion spectroscopy (EDS) to identify the elemental composition of the media, and FTIR to identify the functional groups present in the media.

3.2. **Methodology**

3.2.1. *Macro-Scale Physical Characteristics*

The green adsorption media mixture used in this study consisted of coconut coir, 3/8" expanded clay aggregate, and 3/8" tire chunk in a 1:1:1 ratio (by volume) mixture. The expanded clay aggregate was obtained from a CEMEX construction materials plant, located near Orlando, FL. The coconut coir was manufactured by Sunleaves™ as a growing medium for hydroponic gardening. The tire chunk was obtained from Global Tire Recycling in Wildwood, Florida. No pre-processing of the media was done before physical or chemical analysis commenced. The media mixture and individual components were

analyzed using ASTM standards to determine their physical characteristics, including dry density (ASTM C29), void ratio (ASTM C29 M-09), porosity, and specific gravity (ASTM D854-92). In addition, the particle size distribution (ASTM C136-01) was obtained for the media mixture. A full definition of the mass/volume relationships provided by these parameters provides information for determining the hydraulic residence time/system flow rate relationship for a sorption media filter in the lab and field settings.

3.2.2. *Imaging and Material Analysis*

SEM imaging was conducted on unprocessed media in order to observe the undisturbed pore structure and physical surface morphology. All imaging for unprocessed media was done on a JEOL JSM-6480 SEM with an accelerating voltage of 15 mV and a magnification of 1200, 500 and 50X with a 0.1 gram sample of each of the media ingredients.

A number of analyses were done for raw, Cu-loaded after adsorption, and Cu-desorbed media to observe the structural and chemical changes in the media after each process. All the raw, Cu-loaded after adsorption, and Cu-desorbed powder samples for coconut coir, expanded clay, tire chunk, and the media mixture were milled, ground, and passed through 300 mesh sieves before analysis. The morphology, particle size distribution, and microstructure of raw, Cu-loaded, and Cu-desorbed samples were also determined using FE–SEM (Hitachi S–4700 II) with a resolution of 0.1 nm. Crystalline structures of adsorbents for raw, Cu-loaded and Cu-desorbed samples were measured by XRD scanned from 10 to 80° (2θ) with a scan rate of 4° (2θ) min^{-1} and monochromatic CuK_{α} radiation (MAC Science, MXP18) at 30 kV and 20 mA and further identified by a computer database system (Joint Committee on Powder Diffraction Standards (JCPDS)). The quantities of carbon, oxygen, sulfur, copper, aluminum, and silicon atoms in raw, Cu-loaded, and Cu-desorbed samples were identified by using energy dispersion spectroscopy (EDS). The average copper metal contents in raw, Cu-loaded, and Cu-desorbed samples

respectively were digested by 01 M HCl/HF$_{(aq)}$ and evaluated using both atomic absorption spectroscopy (AAS, GBC model 908) and induced couple plasma/mass spectroscopy (ICP/MS, ELAN model 5000) for double check averagely. Each calibration curve was generated with its corresponding standard metal solution at ten different concentrations and that generated the expected Cu metal concentrations in the raw, Cu-loaded, and Cu-desorbed samples, respectively. Infrared spectra of the raw, Cu-loaded, and Cu-desorbed samples were prepared mixed with KBr in powder sample discs and were recorded and calculated on a Varian 1000 Digilab FTIR spectrometer of Attenuated Total Reflectance (ATR) with fully computerized data storage and data handling capabilities over the range 4000–400 cm^{-1}. For all spectra reported, a 64-scan data accumulation was conducted at a resolution of 4 cm^{-1}.

3.3. <u>Results and Discussion</u>

3.3.1. *<u>Macro-Scale Physical Characteristics</u>*

A summary of the physical characteristics of the adsorption media that describe the macro pore structure and the methods used to determine them are found in Table 3.1. It can be seen that the density and porosity of the mixture is heavily influenced by the physical properties of the expanded clay and tire chunk, while the coconut coir is considerably less dense and more porous than the expanded clay and tire chunk at the macro scale. This would make it more cost-effective on a weight basis, however the higher porosity could allow larger particulate matter to travel deep into the filter media, causing potential clogging issues. The particle size distribution for the media mixture, as shown in Figure 3.1, reveals that it has a relatively large median particle size (D50) of approximately 7.5 mm, and 89% of particles are retained above the no. 4 (4.75 mm) sieve. Additionally, the media mixture is non-uniformly distributed (poorly graded) with a coefficient of uniformity, Cu, of approximately 1.75 and coefficient of curvature, Cc of approximately 0.97.

Table 3.1 Macro-scale physical properties of the green adsorption media.

Characteristic	Expanded Clay	Tire Chunk	Coconut Coir	Mixture
Dry Density (kg·m³)	600.29	506.16	113.10	429.05
Void Ratio	0.58	0.57	0.91	0.61
Porosity	0.37	0.36	0.48	0.38
Specific Gravity	1.42	1.17	1.06	1.11
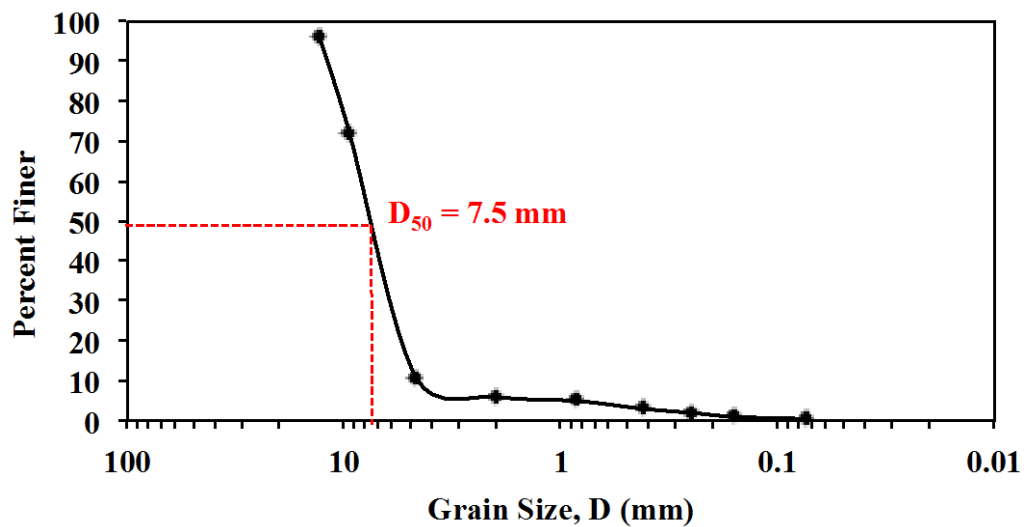
Figure 3.1. Particle size distribution for the adsorption media mixture.

3.3.2. *SEM Imaging*

The SEM microphotographs presented in Figure 3.2 shows the surface morphologies of the three media prior to adsorption. Both the coconut coir and expanded clay exhibit a network of inner pores that would provide greater surface area for adsorption, although the coconut coir appears to have a more extensive and homogenous inner pore network. The surface of the tire chunk is relatively homogeneous with no visible inner pore network, suggesting that it has less surface area available for adsorption, and hence fewer sites for adsorption.

53
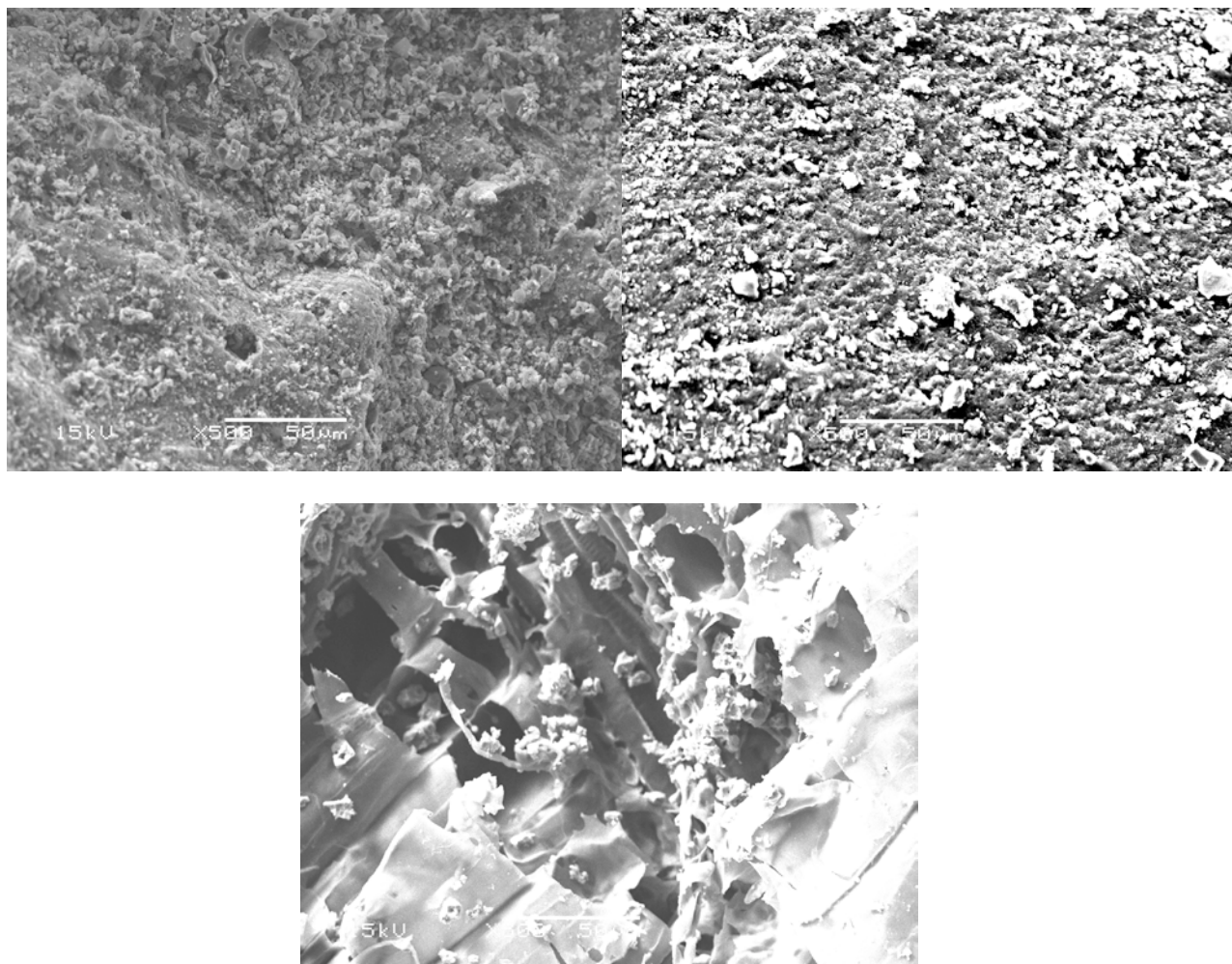
Figure 3.2. SEM images of the undisturbed surface structures of the (a) expanded clay, (b) tire chunk, and (c) coconut coir at 500X magnification

The FE-SEM microphotographs shown in Figure 3.3 were used to investigate the morphologies, crystallinity, and microstructures of the raw (A), Cu-loaded (B), and Cu-desorbed (C) samples, consisting of the media mixture, tire chunk, expanded clay, and coconut coir materials, respectively. As shown in Figure 3.3(A)-(a), the adsorption media mixture mixed with 1:1:1 volume ratio of tire chunk, expanded clay, and coconut coir has an irregular shape with average diameters of approximately 0.5–15 μm.

Similarly, the particle size of Cu-loaded/Cu-desorbed media mixture was around 1−8 μm, as identified by the FE-SEM micrograph shown in Figure 3.3(B,C)-(a). The media mixture was well dispersed with irregular shapes and sizes after the adsorption/desorption removal process of copper contaminants. From Figure 3.3 (A)-(b), it has been recognized that milled or ground tire chunk after a pretreated process has 60–90 nm in diameter and 150–350 nm in length ultrafine particles well-dispersed on the surface of pretreated tire chunk. Additionally, it can been seen that aggregated ultrafine ZnO particles or carbon black powders may be reformed by heat effects in the process of milling or grinding. After the adsorptive removal and desorption processes of copper-contaminated wastewaters, it was also well- dispersed with irregular shapes and sizes around 1−12 μm identified by FE−SEM micrograph shown in Figure 3.3(B,C)-(b). Interestingly, there are no structural changes or damages between adsorption/desorption processes of copper-contaminated wastewaters onto tire chunk using 0.1M HCl as a desorbing agent, observed in Figure 3.3(A,C).

According to the FE-SEM microphotos, there are significant morphological differences between the raw expanded clay and Cu-loaded/Cu-desorbed expanded clays after the adsorptive removal process of copper-contaminated wastewaters, which are observed in Figure 3.3(A)-(c) and Figure 3.3 (B,C)-(c), respectively. The irregular shapes of crystals and notably aggregated ultrafine particles around 2−10 μm diameter of SiO_2 mixed with Al_2O_3 green adsorbents are found in Figure 3.3(A)-(c). The Cu-loaded/Cu-desorbed expanded clays were well dispersed with irregular shapes and sizes around 0.5−10 μm, identified and shown in Figure 3.3 (B,C)-(c). Furthermore, FE-SEM analyses reveal that the SiO_2/Al_2O_3 ultrafine particles are highly mixed and dispersed. Interestingly, it is also shown that the ultrafine particles of SiO_2/Al_2O_3 mixtures were not all separated, but the sizes narrowly distributed, which might be resulting from van der Waals' force attraction of the ultrafine particles. Figure 3.3(A)-(d) confirms that the rough surface of coconut coir material is favorable for adsorptive removal of copper. This observation is

consistent with the result of the EDS measurement represented in Table 3.2. In addition, notably

visualized spherical or irregular shaped CuO ultrafine particles with a diameter of approximately 100–250

nm were found as shown in Figure 3.3(B)-d). Figure 3.35(C)-(d) showed that the CuO ultrafine particles

were possibly digested and washed out from the surface of pore structures in the desorption process using

0.1M HCl.
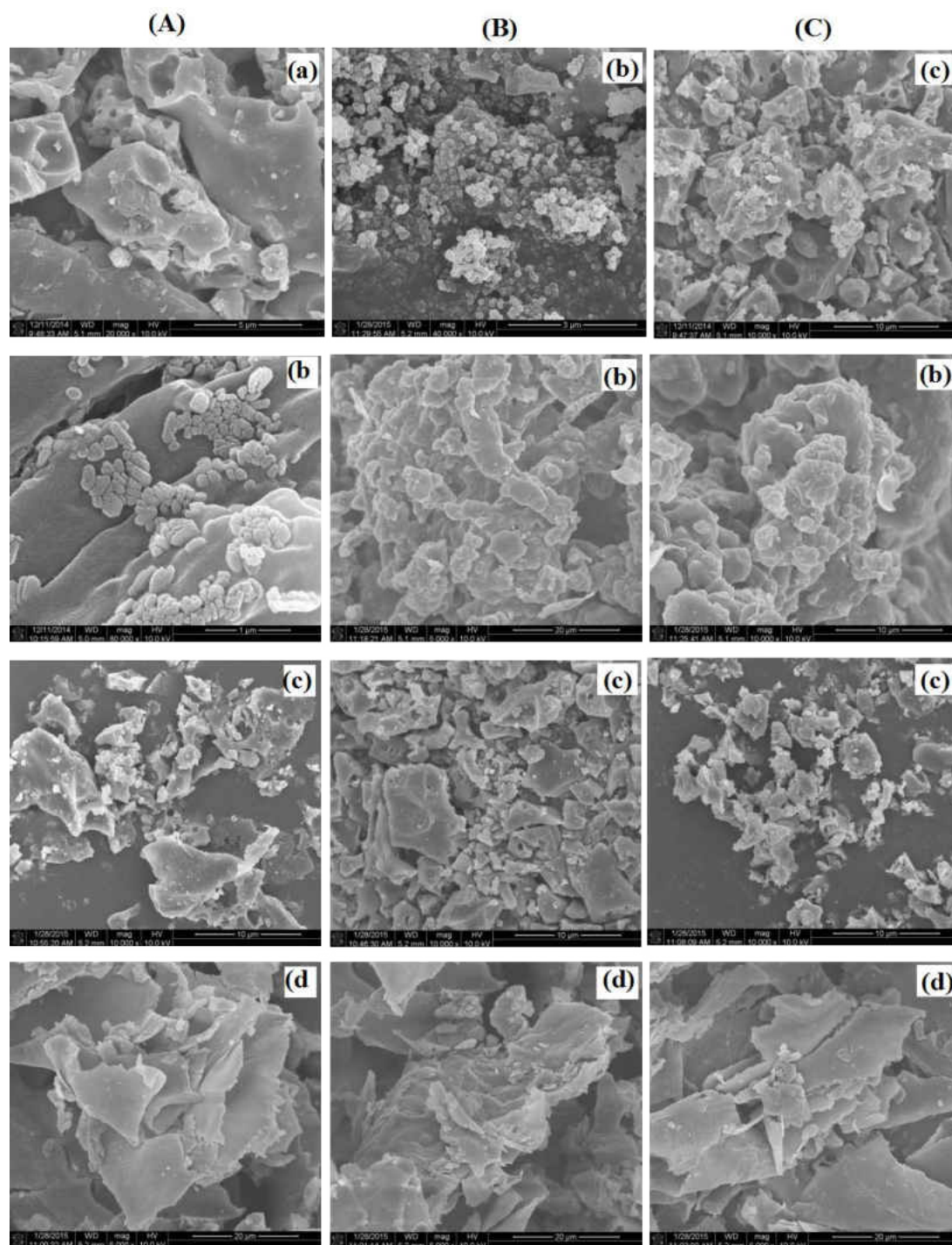
Figure 3.3. FE-SEM micrographs of (A) raw, (B) Cu-adsorbed, and (C) Cu-desorbed powder samples for (a) media mixture, (b) tire chunk, (c) clay, and (d) coconut coir green adsorption media.

57

3.3.3. *XRD Crystalline Structure Analysis*

Powder X-ray diffraction analyses of the porous adsorption materials were performed to confirm the crystalline phases in the media mixture, tire chunk, expanded clay, and coconut coir materials. The XRD patterns of raw and Cu-loaded/Cu-desorbed media mixture and expanded clay are plotted in Figure 3.4(a) and Figure 3.4(c), respectively. Both raw and Cu-loaded/Cu-desorbed expanded clay is crystalline as it shows sharp diffraction peaks. The intensive peaks appearing at 2θ angles in the XRD patterns of raw and Cu-loaded expanded clay are characteristics of crystalline materials. It can be seen that the fine structure remains stable and similar after the copper adsorption/desorption processes. It was observed that the diffraction peaks for both raw and Cu-loaded/Cu-desorbed expanded clay corresponded to hexagonal-typed SiO_2 of (100), (011), (110), (112), (121), (440) (JCPDS file No.74-1811) and monoclinic-typed Al_2O_3 of (400), (310), (511), (113) (JCPDS file No. 86-1410) as well the peaks for the raw and Cu-loaded/Cu-desorbed media mixture. Based on the intensities of XRD patterns of raw and Cu-loaded/Cu-desorbed mixture or expanded clay, the major component appears to be SiO_2. Both raw and Cu-loaded/Cu-desorbed samples are crystalline as they show sharp diffraction peaks, and the position and relative intensity of the diffraction peaks of the samples match well with the standard XRD data for hexagonal-typed SiO_2 and monoclinic-typed Al_2O_3. Moreover, the intensive peaks appearing at 2θ angles in the XRD pattern of hexagonal-typed SiO_2 and monoclinic-typed Al_2O_3 are characteristics of these materials, which possess numerous pores or cavities where copper species can be easily exchanged on the surface. The average crystallite size of expanded clay is calculated to be 150-250 nm using the Scherrer formula from the hexagonal-typed SiO_2 (011) plane (which corresponds the strongest peak). Obviously, there are no structural changes or damages between the adsorption and desorption processes of copper-contaminated wastewaters onto expanded clay/media mixture using, 0.1M HCl as a desorbing agent, as observed in Figure 3.4(a) and Figure 3.4(c), respectively.

The XRD patterns of raw and Cu-loaded/Cu-desorbed tire chunk and coconut coir adsorption media are shown in Figure 3.4(b) and Figure 3.4(d), respectively. These patterns show a broad and less intensive peak around $2\theta = 20\text{-}22°$, which can be attributed to the graphitic structure of activated carbons generated from pretreated tire chunk and coconut coir wastes. The observed 2θ angles are also characteristics of micro- or meso-porous materials of tire chunk and coconut coir, which possess numerous tiny pores or cavities. With the additives of sulfur and ZnO, which improve the hardness and abrasion of tires, bonded ZnS and ZnO particles were observed in the framework of the tire chunk. In addition, the other eleven peaks could be indexed to the (100), (101) of hexagonal-typed ZnS (JCPDS file No.80-0007), (100), (002), (101), (102), (110), (103), (112) of hexagonal-typed ZnO (JCPDS file No. 36-1451) and (111), (022) planes of monoclinic-typed CuO particles (JCPDS file No.48-1548), respectively. The calculated mean particle size of the loaded ZnS, ZnO, and CuO particles by Scherrer equation were about 115, 155, and 130 nm (which corresponds the strongest peak of (100), (101)) or (111)), respectively.

As shown in Figure 3.4(d), it is suggested that CuO was finely dispersed on the surface of coconut coir. It also suggests that after pretreatment there were not enough enhancements in the crystal and pore structures. On the other hand, it proves that CuO particles in as-synthesized Cu-loaded coconut coir were not highly crystalline and ultrapure. Interestingly, the samples have been pretreated under lower milling and grinding temperatures, thus Cu_2O or CuS by-products should not be formed. As such, the diffraction peaks cannot categorically reveal the existence of Cu_2O or CuS peaks. All the pretreated samples indicate similar diffraction lines and intensities at identical 2θ values. The copper species exchanged in pretreated coconut coir was confirmed by the XRD pattern represented in Figure 3.4(d) and the residue was CuO mixed onto the surface of coconut coir. It also showed that the CuO ultrafine particles were possibly digested and washed out from the surface of pore structures in the desorption process. The results are consistent with the data of FE-SEM microphotos shown in Figure 3.4(d).
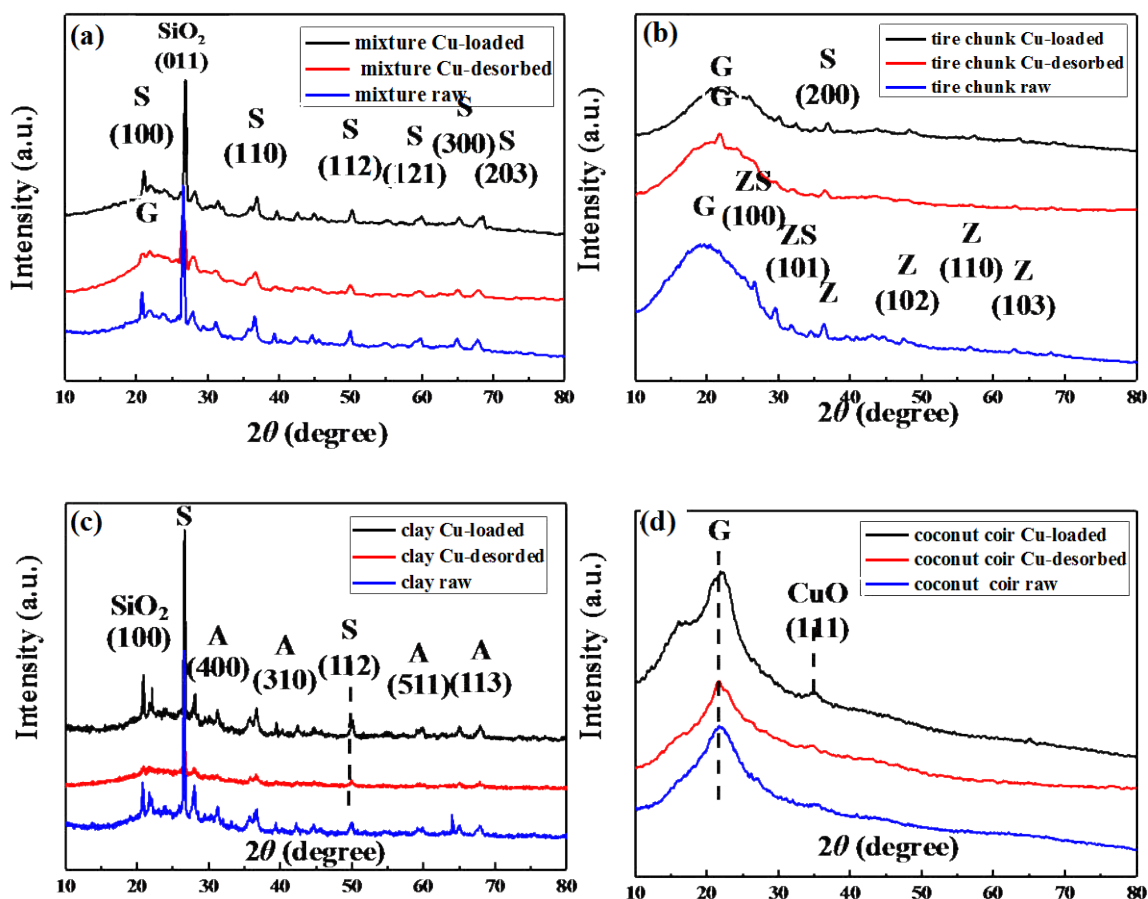
Figure 3.4. XRD patterns of (a) media mixture (S: SiO_2; A: Al_2O_3), (b) tire chunk (G: graphite; ZS: ZnS; Z: ZnO), (c) expanded clay (S: SiO_2; A: Al_2O_3), and (d) coconut coir (G: graphite) for the raw, Cu-loaded or Cu-desorbed samples.

3.3.4. *FTIR Analysis*

Generally, FTIR can provide the chemical properties of organic functional groups on the surface of media mixture, tire chunk, expanded clay, and coconut coir for the raw, Cu-loaded or Cu-desorbed samples. Based on the media mixture containing tire chunk, expanded clay, and coconut coir, the specific functional groups such as S-H, O-H, C=O were found in Figure 3.5(a). Since the tire chunk composites

60

are generally mixed with the additives of sulfur powders, which can improve the hardness and abrasion of tires, S-H and C=S bonding were observed in the framework of the tire chunk shown in Figure 3.5(b). From the XRD patterns of expanded clays shown in Figure 3.5(c), hexagonal-typed SiO_2 and monoclinic-typed Al_2O_3 are characteristics of these materials, Figure 3.5(c) indicated that Si-O and Al-O bonds were found on the surface of expanded clays. Based on the porous and amorphous properties of coconut coir, it can be seen that the moisture and organic functional groups such as O-H, C=O, C-H bonding were observed in Figure 3.5(d). Notably, there are not significant changes on the surface during adsorption/desorption processes of Cu-contaminated wastewaters onto coconut coir samples using HCl as a desorbing agent, observed in Figure 3.5.
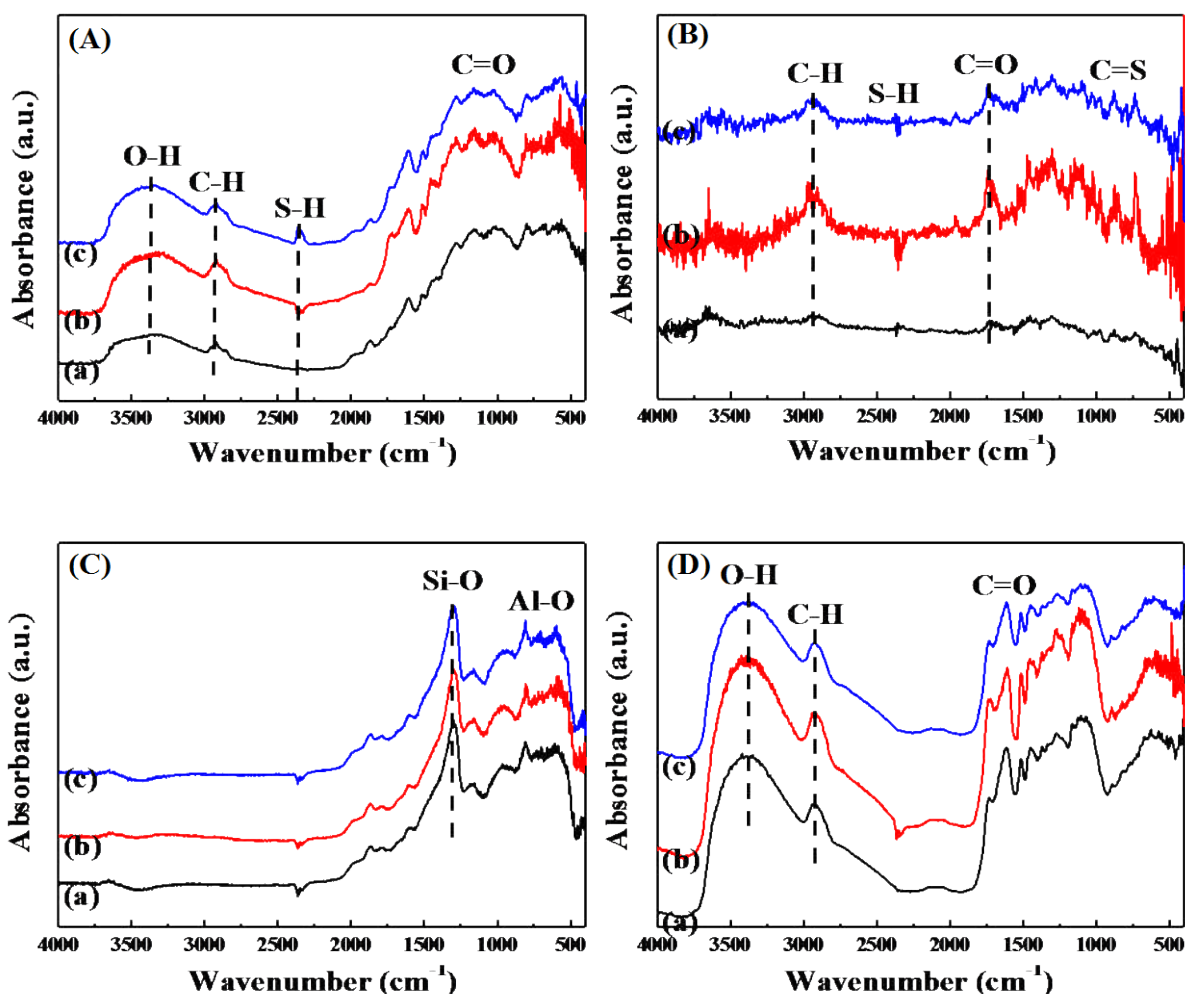
Figure 3.5. FTIR absorbance spectra of (a) raw (fresh), (b) Cu-Loaded, and (c) Cu-desorbed samples for (A) media mixture (B) tire chunk, (C) expanded clays, and (D) coconut coir.

3.3.5. *Elemental Composition Analysis*

Table 3.2 displays the results of elemental analyses of the media mixture, tire chunk, expanded clay, and coconut coir by using average values of EDS/ICP-MS/AA, respectively, where carbon constituents are the main component of typical tire chunk and coconut coir adsorbents. Low metal species and high sulfur content in tire chunk and mixture are also notably found. Moreover, silicon and oxygen

are the main components in the expanded clay adsorbent and trace copper species are present in both Cu-loaded expanded clay and tire chunk adsorbents, respectively. On the contrary, the Cu contents in Cu-loaded mixture and coconut coir adsorbents are 0.4 and 2.81% (atom), respectively. It can be seen that the copper species are loaded or bonded on the hydrophilic surface of coconut coir due to the combination of ion exchange with -OH and -COO functional groups and electrostatic attraction onto a higher specific surface area (Acheampong et al., 2011; Li et al., 2015). Based on the electrostatic attraction (e.g. –OH) and ion exchange effects, expanded clay adsorbents have shown copper sorption occurs in the process of adsorption. Similarly, tire chunk adsorbents also have trace adsorption capacities and sorption occurs primarily through ion exchange or possibly bonding with sulfur atoms (Cu-S) on the hydrophobic surface of the adsorbent framework (Calisir et al., 2009). In addition, it was also found that the higher concentration of copper loaded in the coconut coir correlates with the higher porosity and void ratio compared with the other adsorbents. Conversely, the concentration of copper species in tire chunk is less compared with that of mixture adsorbents due to the effects of lower porosity and void ratio. In the desorption process, the media mixture and coconut coir still have copper contaminated residues in the frame structures that may not be removed during the desorption procedures. These results are consistent with the data shown in Figure 2.3. Comparing the copper adsorption and desorption processes, it is likely that different desorbing agents of DI water, HCl, HNO_3, and H_2SO_4 are also a dominant factor here. It may be due to at least two possibilities; (1) acidic desorption agents may remove and leach out the Cu-contaminants inside or bonded with the surface of these green adsorbents; (2) the hydrophobic or hydrophilic surface properties of the green adsorbents that may affect the wetting abilities of the surface for removing copper contaminant. Based on the comparison in Table 3.2, increasing percentages of oxygen atoms and decreasing copper, silicon, aluminum or sulfur atoms during the desorption process using acidic desorption agents were found. It has been generally suggested that acidic desorption agents are more suitable for the application on the desorption processes of copper-contaminated wastewaters.

63

Table 3.2. Ultimate analyses of raw, Cu-loaded after adsorption, and Cu-desorbed powder samples for media mixture, tire chunk, expanded clay, and coconut coir using average values of EDS/ICP-MS/AA, respectively (variation of ± 0.03 atom%).

Adsorbent	Carbon (atom%)	Oxygen (atom%)	Aluminum (atom%)	Silicon (atom%)	Copper (atom%)	Sulfur (atom%)
Mixture						
Raw	30.31	42.42	6.69	20.03	N.A.	0.55
Cu-loaded	30.46	42.36	6.82	19.90	0.04	0.42
Cu-desorbed	30.30	42.48	6.67	20.01	0.02	0.52
Expanded clay						
Raw	N.A.	45.68	11.66	42.66	N.A.	N.A.
Cu-loaded	N.A.	45.52	11.29	43.10	<0.01	N.A.
Cu-desorbed	N.A.	47.59	10.93	41.48	N.A.	N.A.
Tire chunk						
Raw	83.80	13.37	N.A.	N.A.	N.A.	2.83
Cu-loaded	83.79	13.36	N.A.	N.A.	<0.01	2.82
Cu-desorbed	83.56	13.77	N.A.	N.A.	N.A.	2.67
Coconut coir						
Raw	66.79	33.21	N.A.	N.A.	N.A.	N.A.
Cu-loaded	65.86	33.33	N.A.	N.A.	2.81	N.A.
Cu-desorbed	65.14	34.01	N.A.	N.A.	0.85	N.A.

Note: "N.A." denotes "not available".

3.4. <u>References</u>

Acheampong, M.A., Pereira, J., Meulepas, R., and P. Lens. 2011. Biosorption of Cu(II) onto agricultural materials from tropical regions. *J. Chem. Technol. Biotechnol* 86: 1184-1194.

Calisir, F., Roman, F.R., Alamo, L., Perales, O., Arocha, M.A., and S. Akman. 2009. Removal of Cu(II) from aqueous solutions by recycled tire rubber. *Desalinisation*. 249: 515-518.

Howe, K.H., Hand, D.W., Crittenden, J.C., Trussell, R.R., Tchobanoglous, G. 2012. "Principles of Water Treatment". Pp 370-384. Hoboken, John Wiley & Sons.

Li, Z., Ge, Y., Ge, and Liang Wan. 2015. Fabrication of a green porous lignin-based sphere for the removal of lead ions from aqueous media. J. Hazard. Mater. 285: 77–83.

Musso, T.B., Parolo, M.E., Pettinari, G., and F.M. Franscisa. 2014. Cu(II) and Zn(II) adsorption capacity of three different clay liner materials. *J. of Environ. Management* 146: 50-58.

Oueslati, W., Ben Rhaiem, H., and A. Ben Haj Amara. 2009. XRD Investigations of hydrated homoionic montmorillonite saturated by several heavy metal cations. *Desalinisation* 271: 139-149.

Sing, K., Everett, D., Haul, R., Moscou, L., Pierotti, R., Roquerol, J., and T. Siemieniewska. Reporting physiosorption data for gas/solid systems. 1985. *Pure and Appl. Chem.* 601: 603-619.

CHAPTER 4:   SCALING ASSESSMENT FOR FIELD IMPLEMENTATION

4.1. Introduction

4.1.1. Background and Literature Review

Design of a cost-effective and reliable sorption media reactor depends on a number of key design variables surrounding both the media characteristics and system operating variables, as illustrated in Figure 4.1. Proper selection of the hydraulic residence time (HRT) and the associated hydraulic loading rate can be difficult and costly with an experimental approach through the use of a series of column breakthrough studies. As a result, it is necessary to develop a more efficient method to optimize the selection of the appropriate HRT.
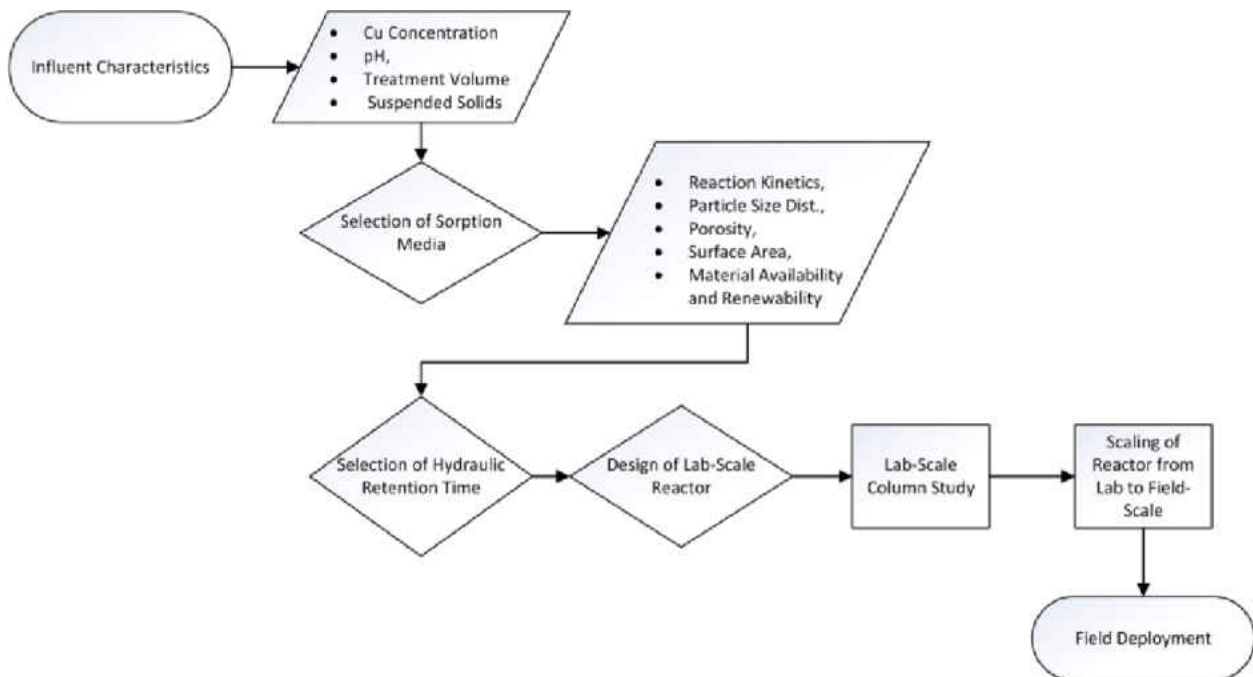
Figure 4.1. Design process for a sorption media reactor

Another challenging design aspect is the proper scaling-up of the reactor from the lab to field scale. Undertaking lab-scale studies, such as column studies, allows for effective design of full-scale sorption media reactors without undertaking full-scale pilot studies that are costly in terms of time and materials. However, care must be taken in scaling-up to a full-scale reactor that similitude can be confirmed; otherwise the adsorbent capacity and breakthrough profile cannot be maintained as expected. Crittenden et al (1986) established an effective method for scaling-up granular activated carbon (GAC) reactors, using dimensional analysis, that has been confirmed by a number of studies (Knappe *et al*., 1997; Cummings *et al.,* 1994; Westerhoff *et al.*, 2005; Corwin and Summers, 2010). This method is based on the dispersed-flow pore and surface diffusion model (DFPSDM) and the 6 independent dimensionless numbers that fully define the phenomenon. However, the key to this method's success involves varying the adsorbent particle size from lab to field scale, which is possible with manufactured sorption materials such as GAC. For green sorption media, however, materials usually cannot be manufactured to specification, thus the same media particle size must be used for small-scale and full-scale reactors, which presents a challenge in scaling-up. Therefore, development of an alternative method is desired in this study for scaling-up of sorption media reactors with respect to a constant media particle size.

The well-known Péclet and Damköhler numbers provide dimensionless parameters for describing and quantifying the relationship between advective and dispersive transport (Péclet) and the relationship between advective transport and reaction rate (Damköhler). They have been useful in describing a number of phenomena in reactive transport in porous media. Werner et al. found a relationship between the Damköhler number and the degree of tailing or fronting of breakthrough curves for organic groundwater pollutants (Werner *et al*., 2012). Golfier et al. (2002) observed a relationship between the Damköhler and Péclet numbers and the regime of wormhole formation during dissolution of a porous medium. Qang et al. found that dominant wormhole formation occurred under high Péclet and Damköhler numbers, while uniform dissolution occurred under low values (Qang *et al.*, 2003). Finally, Fredd and Fogler (1998)

observed an optimum Damköhler number for dominant wormhole formation, which could be related to an optimal injection rate for porous medium dissolution.

Aqueous copper transport through a sorption media reactor can be described as reactive transport through porous media. Numerous approaches have been taken for modeling reactive transport in porous media at different scales, including pore-scale (Qang *et al.*, 2002; Qang *et al.*, 2006), macroscopic, or Darcy scale (Steefel, 2008; Golfier *et al.*, 2002), and multi-scale approaches (DeLima *et al.,* 2010). For design of a sorption media reactor, understanding the relative influence of each scale and determining which scale is rate-controlling under a given flow scenario is critical. This includes the pore scale, where the adsorption reaction rate and rate of diffusion are of interest, and the macroscopic/Darcy scale, where the advective transport rate and hydrodynamic dispersion are of interest.

4.1.2. *Chapter Objectives*

This work in this chapter aims to expand the application of the Péclet and Damköhler numbers to sorption media reactor design by developing a relationship between the Damköhler number and copper adsorption in a sorption media reactor, leading to the development of a new scaling-up method using these dimensionless numbers to aid in copper removal. The study objectives are achieved through conducting a series of breakthrough studies at different hydraulic loading rates on the sorption media mixture consisting of 1/3 expanded clay aggregate, 1/3 recycled tire chunk, and 1/3 coconut coir, by volume. The Damköhler and Péclet numbers are then calculated for the various hydraulic loading rates. From this, a relationship is derived between the Damköhler number and the copper removal efficiency of the media, in order to identify the optimal HRT for adsorptive copper removal. Finally, a method of scaling-up sorption media reactors from lab-scale to field scale with a constant particle size is presented through a dimensional analysis involving the Péclet and Damköhler numbers.

4.2. <u>Methodology</u>

4.2.1. *Column Breakthrough Study*

The column breakthrough tests were set-up as an upward-flow system with three Plexiglas columns with a diameter of 5.08 cm (2.0 inches) and a length of 30.48 cm (1.0 ft) as shown in Figure 2. The columns each contained 350 g of sorption media, which was oven-dried at 75 C for a minimum of 36 hours to eliminate biotic activity and to ensure only physiochemical reactions took place. In addition, glass beads and filter fabric were provided at the bottom of the columns to assist in dispersion, and filter fabric was provided at the top of the columns to prevent outward flow of fine particles. The influent was delivered to the columns by a Masterflex L/S peristaltic pump with Masterflex no.16 tubing. The three columns were exposed to identical influent conditions and flow rates, to provide triplicate measurements for each test.

To establish the adsorption capacity and removal efficiency of the sorption media with different hydraulic loading rates, a series of tests were run with varying theoretical hydraulic retention times (HRTs) of 12, 18, 24, 30, and 39 minutes. The influent conditions were held constant for each scenario with a concentration of 1 mg·L^{-1} Cu and a pH of 3.75. The influent was prepared by spiking single-distilled water with Fisher Scientific 1000 ppm copper standard solution. Distilled water was used as the liquid matrix to ensure that only sorbate/sorbent reactors were occurring. Effluent concentrations were analyzed using the United States Environmental Protection Agency (USEPA) Bicinchoninate method no. 8506 and a HACH DR 2800 spectrophotometer. From the experimental data, breakthrough curves (BTCs) were developed to provide direct comparison between the flow scenarios and to quantify the difference in copper removal. The Modified Dose-Response (MDR) model, described in Section 2.2.6 was employed to develop the BTCs.

To confirm that there is a significant difference between the resulting BTCs generated under the varying HRTs, a two-tailed t-test on a normal regression analysis was used to compare the individual column tests. The raw data from each column test were first linearized by plotting $\ln[(C_o/C_e) -1]$ vs. t (time). Then, they were fit to the linear regression model in equation (23) which was used to compare the differences in the adsorption curves generated by the different HRTs:

$$\hat{y} = \beta_0 + \beta_1 x_1 + \beta_2 x_2 + \beta_3 x_1 x_2 \tag{22}$$

where $\hat{y}$ is the predicted $\ln(C_o/C_e-1)$, x_1 is time (minutes), and x_2 is an indicator variable.

To determine the difference between the 12 minute HRT and 18 minute HRT for example, the indicator variable, x_2, that takes on the value 1 when the HRT is 12 minutes and takes on the value 0 if the HRT is 18 minutes. Consequently, the linear model used for prediction is $\hat{y} = \beta_0 + \beta_2 + (\beta_1 + \beta_3)x_1$ when the HRT is 12 minutes, and otherwise, the prediction is $\hat{y} = \beta_0 + \beta_1 x_1$ when the HRT is 18 minutes. The same methodology was used to compare each of the possible combinations, bringing the total number of comparisons to 10.

To compare the slopes of the linear equations which were developed, the null hypothesis, H_0 is that $\beta_3 = 0$ and the alternative hypotheses, H_1 is that $\beta_3 \neq 0$. Thus, if the null is rejected, the regression parameter representing the slopes of the line are significantly different. Each analysis was considered statistically significant at a confidence level of 95% ($\alpha=0.05$). The P-value results from the two-tailed t-test indicate if there is significant difference in the slope of the copper adsorption curves being compared. Statistical analyses were performed using R statistical software (2013).

4.2.2. *Péclet Number Calculations*

To discover whether advective transport or dispersion/diffusion is dominant at the scale used for the column breakthrough study, the Péclet number was calculated. For this study, the Péclet number is defined in two forms, the dispersive Péclet number, which is the ratio of the advective transport rate to the hydrodynamic dispersion rate, and the diffusive Péclet number, which is the ratio of the advective transport rate to the molecular diffusion rate (Steefel, 2008). Calculation and comparison of the two Péclet numbers at the same representative length scale reveals if mechanical dispersion dominates the overall dispersion or if molecular diffusion must be considered in the scaling process. The dispersive and diffusive Péclet numbers are given as:

$$Pe_{disp} = \frac{Advective\,Transport\,Rate}{Hydrodynamic\,Dispersive\,Transport\,Rate} = \frac{ul}{D_h} = \frac{u(u\tau)}{D_h} = \frac{u^2\tau}{D_h} \tag{23}$$

$$Pe_{diff} = \frac{Advective\,Transport\,Rate}{Molecular\,Diffusive\,Transport\,Rate} = \frac{ul}{D_m} \tag{24}$$

where u (cm·s^{-1}) is the interstitial velocity, defined as the flow rate per unit area divided by the porosity, τ (s) is the residence time in the system, D_h (cm^2·s^{-1}) is the hydrodynamic dispersion coefficient, l is the characteristic length scale which is taken to be the average fixed-bed length from the column study, 29.9 cm, and D_m is the molecular diffusion coefficient which is taken to be $7.33*10^{-6}$ cm^2·s^{-1} for Cu^{2+} (Lasaga, 1998). The interstitial velocity and residence time are known from the column study, while the hydrodynamic dispersion coefficient is determined experimentally.

The hydrodynamic dispersion coefficient accounts for both molecular diffusion and mechanical dispersion and is defined as the sum of the molecular diffusion and mechanical dispersion coefficients:

$$D_h = D_m + D_d \tag{25}$$

It has been established (Lasaga, 1998) that D_d is proportional to the interstitial velocity of the fluid. Thus, if radial dispersion is neglected, such that only longitudinal dispersion is considered then the mechanical dispersion coefficient takes the form:

$$D_d = \alpha_L u \tag{26}$$

where α_L (cm) is the longitudinal dispersivity of the media. Thus, it can be seen that at higher velocities, $D_d \gg D_m$, thus the effects of molecular diffusion can be ignored and D_h reduces to $\alpha_L u$.

The hydrodynamic dispersion coefficient was estimated by conducting a tracer study on the media mixture. The tracer study was set up similar to the column study, with a single Plexiglas column of 5.4 cm diameter and 35.8 cm length. The sorption media was packed throughout the length of the column. A 2 mL pulse of rhodamine WT tracer was injected through the media filled column under a constant flow rate of tap water, and the effluent concentration was periodically measured at the top of the column using an *Aquaflor* handheld flourometer. The flow rates in the tracer study were adjusted to provide the same theoretical interstitial velocities that occurred in the column breakthrough studies. A rhodamine WT BTC was then developed and the method of temporal moments was used to calculate the coefficient. Applying this method, the hydrodynamic dispersion coefficient is calculated as (Weihermuller *et al.*, 2011):

$$D_h = \frac{v^3}{2z}(\mu_2 - \mu_1^2) \tag{27}$$

where z (cm) is the distance from point of injection to point of sampling (35.8 cm), μ_1 (s) is the first temporal moment of the distribution, μ_2 (s^2) is the second temporal moment of the distribution, and v (cm·s^{-1}) is the pore water velocity (Pang *et al.*, 2003);

$$v = \frac{z}{\mu_1 - 0.5{t_0}^2} \tag{28}$$

where t_0 (s) is the duration of tracer injection, which is negligible for a pulse tracer. The first and second temporal moments are calculated by equations (30) and (31), respectively from the tracer BTC.

$$\mu_1 = \frac{\sum_0^{n-1} t_i \frac{(C_i + C_{i+1})}{2} \Delta t}{\sum_0^{n-1} \frac{(C_i + C_{i+1})}{2} \Delta t} \tag{29}$$

$$\mu_2 = \frac{\sum_0^{n-1} t_i^2 \frac{(C_i + C_{i+1})}{2} \Delta t}{\sum_0^{n-1} \frac{(C_i + C_{i+1})}{2} \Delta t} - \mu_1 \tag{30}$$

4.2.3. *Damköhler Number Calculations*

Aqueous chemical reactions in porous media are rate-limited by either fluid transport (transport-scale) or surface reactions between the fluid and solid (reaction-scale). When the concentration in the aqueous phase of the constituent of interest reaches equilibrium over a defined spatial domain, the rate of reaction is considered to be transport-controlled (Steefel, 2008). The Damköhler number, a transport parameter defined as the ratio between the chemical reaction rate and the advective transport rate, provides an indication as to whether constituent transport or surface reactions on the media is the rate-limiting factor. Its definition depends on the spatial and temporal scale of interest. For the case of adsorption within a porous media column, the spatial scale is defined by the length of the fixed bed, and the temporal scale is defined by the hydraulic loading rate. By this definition, the Damköhler number is given as:

$$Da = \frac{ReactionRate}{AdvectiveTransportRate} = \frac{C_0^{p-1}kl}{q} \qquad (31)$$

where k is the reaction rate constant, C_0 (mg·L^{-1}) is the influent concentration, p is order of reaction

(dimensionless), l (cm) is the fixed-bed length from the column study and q (cm·min^{-1}) is the hydraulic

loading rate.

The Damköhler number was computed for the sorption media mixture for each of the 5 column

scenarios to compare the effects of hydraulic loading rate on the reaction-transport relationship. An

influent concentration of 1.0 mg·L^{-1} was used for all calculations, consistent with the influent

concentration used in the column breakthrough studies. The reaction rate constant, k was taken to be the

second-order rate law coefficient, 0.114 g·mL^{-1}·min^{-1}, as determined by the kinetic study results presented

in Section 2.3.2.

4.3. Results and Discussion

4.3.1. Column Breakthrough Study

The data from the five column test scenarios were fit to the linear for of the MDR model, by

using linear regression, to obtain the model equation and parameters. The results showed that the MDR

model described the breakthrough curves quite well, with R^2 values all above 0.94, as shown in Table 4.1.

The tests were not carried completely to breakthrough ($C_e/C_0 = 1$), as they reached asymptotic rates of

removal over time (Figure 4.2). As was hypothesized in Section 2.3.4, either there is a shift in the

adsorption rate due to the higher-energy sites being used up in the initial time period, or that the

adsorptive capacity of the media mixture has been reached and removal is occurring through metal

hydroxide precipitation. As a result of the asymmetric nature of the BTC, linear regression was only

carried out over the range of data where the effluent concentration was increasing with time, providing a conservative estimate of the actual adsorption capacity.

Table 4.1. Summary of the Modified Dose-Response (MDR) parameters obtained from the column adsorption study

Theoretical HRT (min)	Hydraulic Loading Rate (cm·min^{-1})	BTC Equation[a]	a_{MDR}	q_0 (mg·g^{-1})	R^2
12	2.49	y = 1.29x – 2.77	1.29	0.025	0.96
18	1.66	y = 1.40x – 3.44	1.40	0.033	0.94
24	1.24	y = 0.60x – 2.69	0.60	0.25	0.98
30	1.00	y = 0.86x – 1.70	0.86	0.021	0.96
39	0.77	y = 0.88x - 2.41	0.88	0.045	0.96

[a]Where $y = ln\ (C_e/(C_0-C_e))$ and $x = ln(C_0Qt)$

(a) 12 min HRT

(b) 18 min HRT

(c) 24 min HRT

76
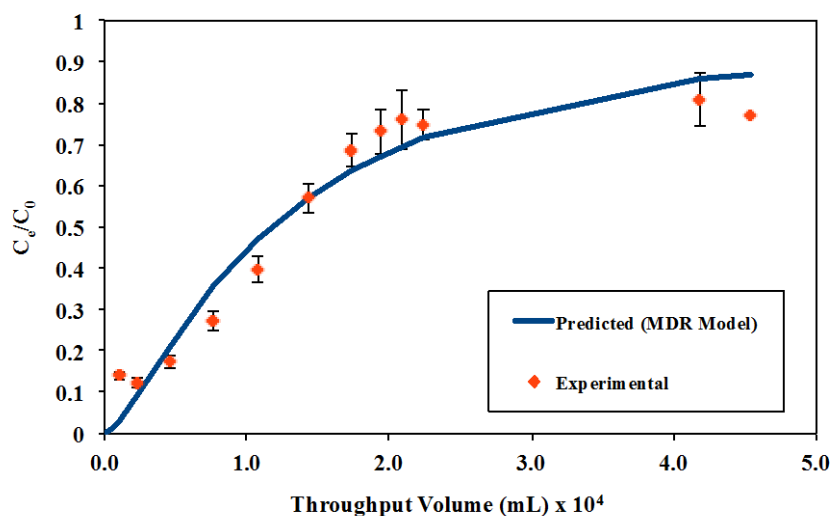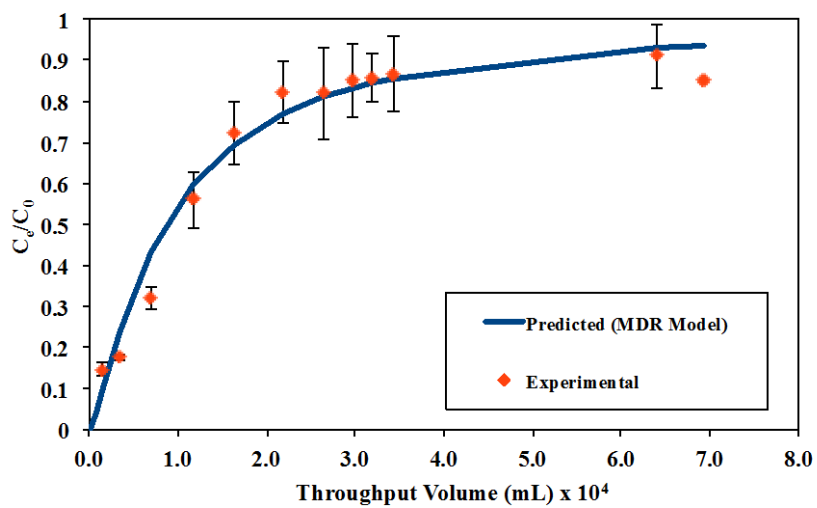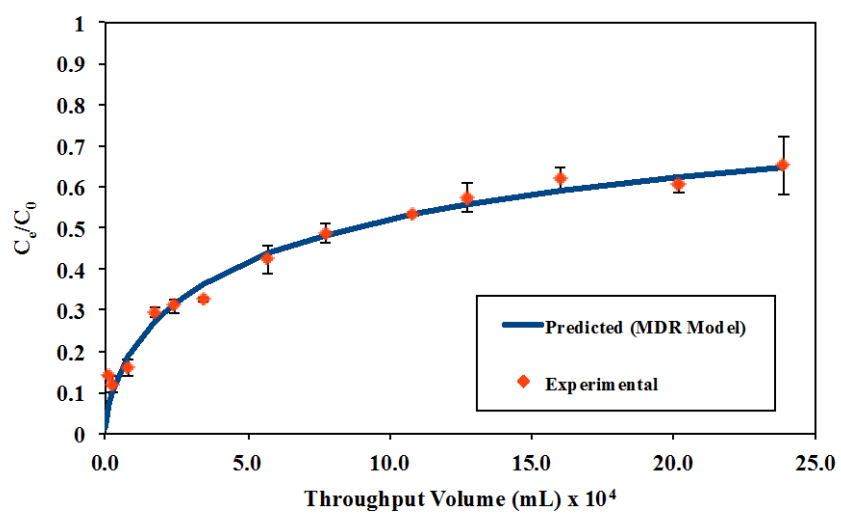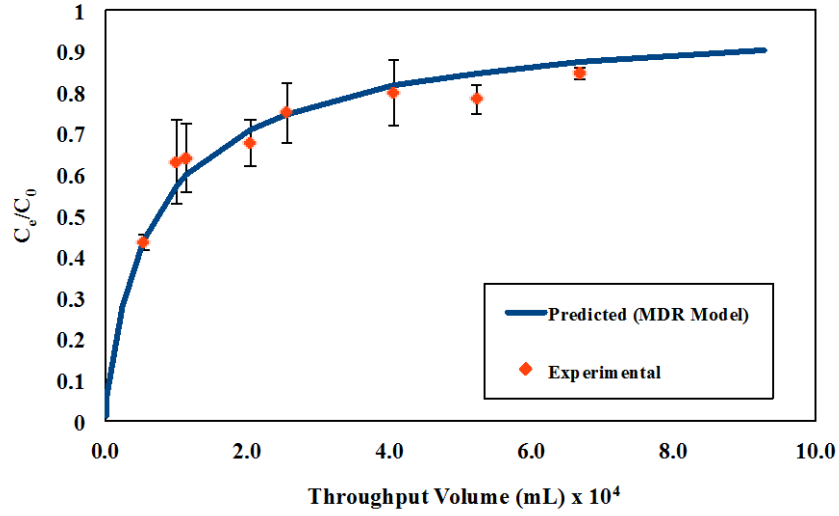
(d) 30 min HRT

(e) 39 min HRT
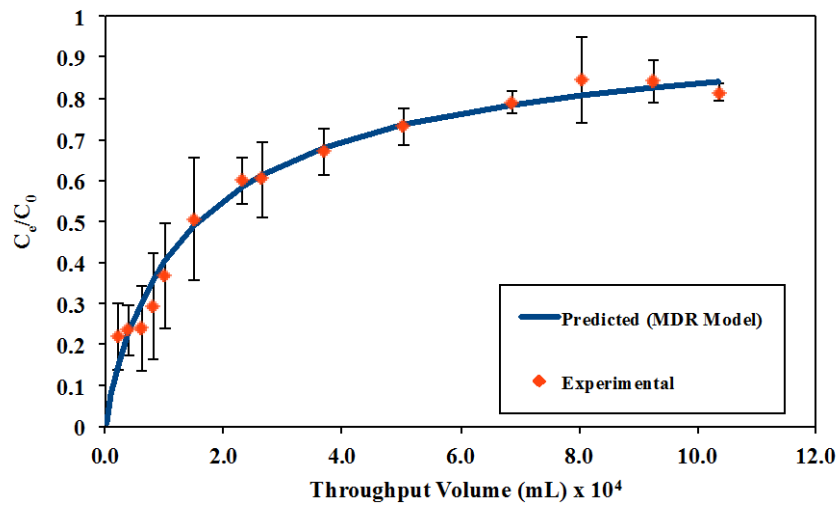
Figure 4.2. Experimental and predicted breakthrough curves for (a) 12 min HRT (b) 18 min HRT (c) 24 min HRT (d) 30 min HRT and (e) 39 min HRT. Experimental data points represent an average of the three column measurements and the error bars represent the standard deviation. It should be noted that the horizontal scales have been adjusted for each curve to account for the duration of the test.

The results in Table 4.1 also show that a peak copper adsorption was observed for the 24 minute HRT, with an equilibrium adsorption capacity of 0.25 mg·g^{-1}. The relationship of the equilibrium adsorption capacity and the flow rate through the column, presented in Figure 4.3 shows that the presence of an optimum flow rate for copper removal is quite salient. Further, the asymptotic values of Ce/C0 vary between the scenarios and their relationship to the flow rate correlates with that of the equilibrium adsorption capacity, with a peak effluent concentration of 0.65 mg·L^{-1} being observed for the 24 minute HRT , compared to 0.91 mg·L^{-1} for the 12 minute HRT. This suggests a similarity between the adsorption reaction rate and the precipitation reaction rate and that both adsorptive and precipitative copper removal are maximized at the 24 minute HRT.
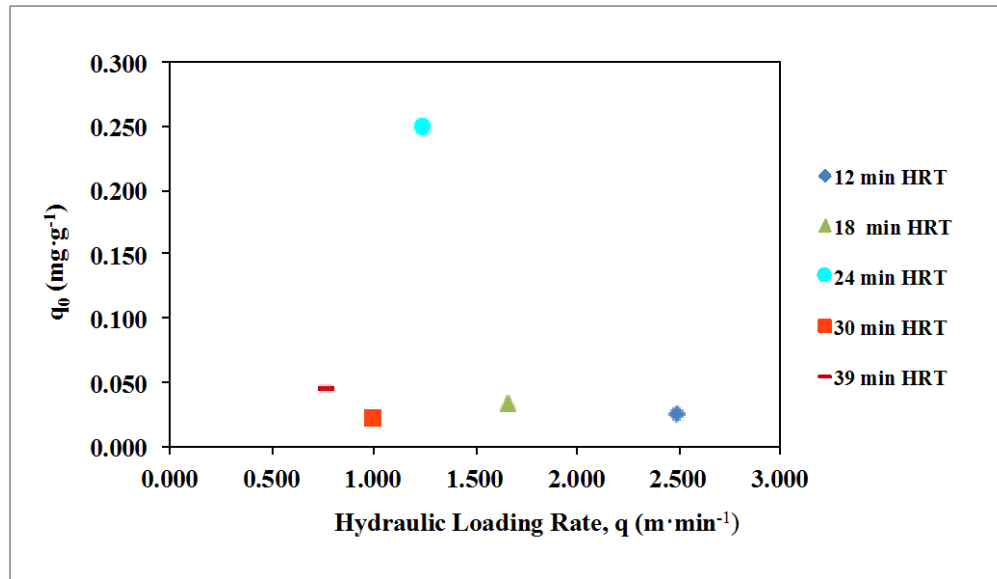
Figure 4.3. Relationship of equilibrium sorption capacity, q_0, and the hydraulic loading rate for the column tests.

In order to make confident conclusions about the media performance under varying HRTs, it is critical to establish a statistically significant difference in the data from the column studies. A comparison between the BTCs of each of the possible HRT combinations was made using a two-tailed t-test based on

the linear regression parameter β3 from (23). Statistically significant differences were found for all HRT comparisons at the 95% confidence level ($\alpha = 0.05$), with the exception of the 12 minute compared to the 18 minute HRT and the 30 min compared to the 39 minute HRT, which exhibited P-values of 0.33 and 0.82, respectively. Physically speaking, this suggests that the media exhibited significantly different adsorption rates over time, when comparing the peak at the 24 minute HRT to only the 18 minute and 30 minute HRTs.

4.3.2. *Péclet Number Calculations*

The BTCs from the tracer study under the 5 HRTs (Figure 4.4) reveal significant skewness. As a result, small amounts of tracer were measured in the effluent long after the peak was observed, and the BTCs for the 24, 30, and 39 minute HRTs were truncated. To obtain better estimates of the BTC moments using equations (30) and (31), the BTCs for the 24, 30, and 39 minute HRTs were extrapolated according to the slope of the tail to a zero concentration point, using the method of Pang *et al*. (2003). Applying the method of moments to the 5 BTCs, hydrodynamic dispersion coefficients (D_h) of 0.23, 0.077, 0.071, 0.081, and 0.038 $cm^2 \cdot s^{-1}$ were obtained for the 12, 18, 24, 30, and 39 minute HRTs, respectively.
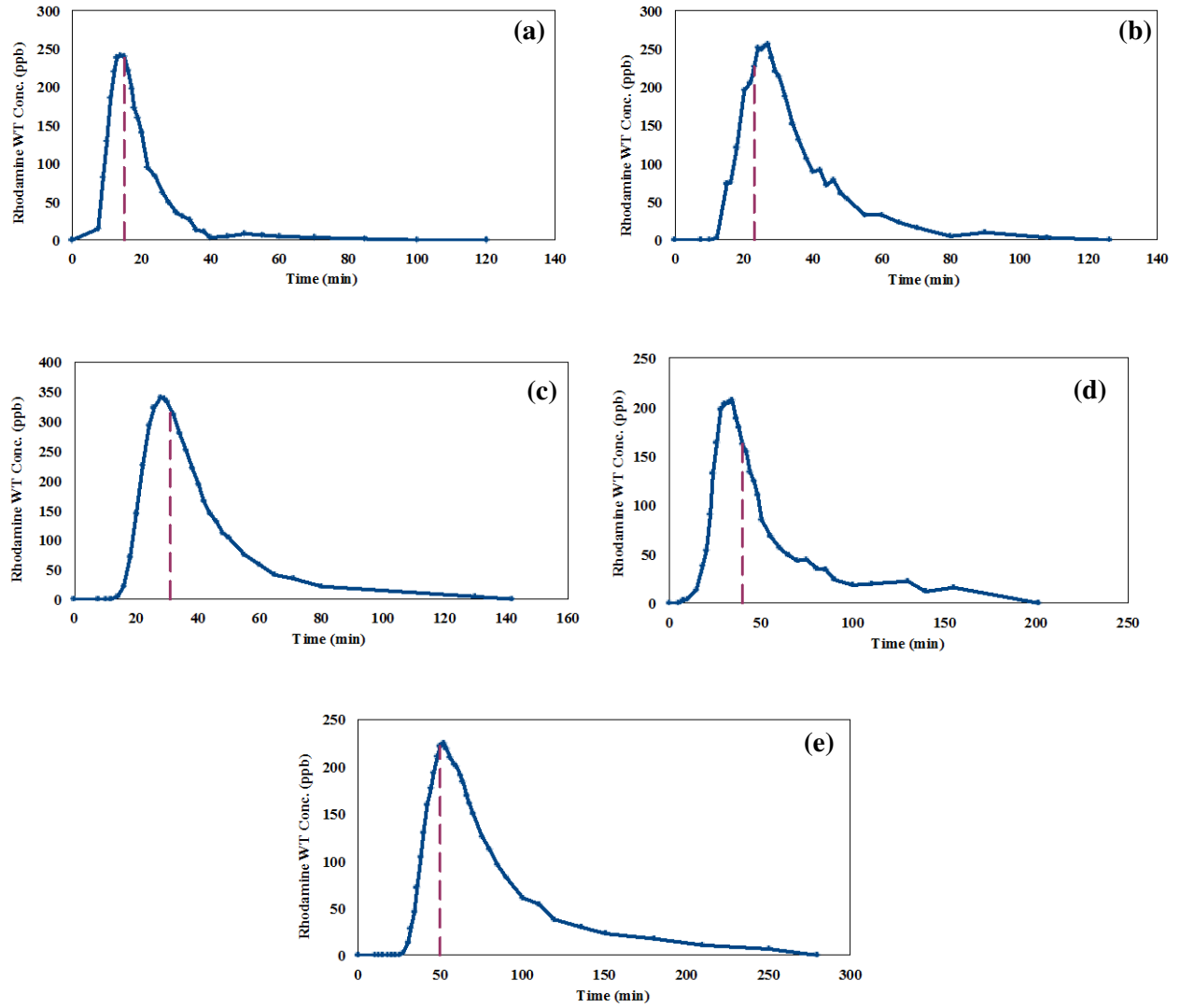
Figure 4.4. Tracer BTCs for the (a) 12 min HRT (b) 18 min HRT (c) 24 min HRT (d) 30 min HRT and (e) 39 min HRT. The theoretical HRT for the tracer column is indicated by the vertical line.

Synthesizing the experimental data from the tracer study and the column study flow parameters, the dispersive (Pe_{disp}) and diffusive (Pe_{diff}) Péclet numbers were calculated and are presented in Table 4.2. The values of Pe_{disp} reveal that the flow regime was slightly advection-controlled, however the values of Pe_{disp} are all on the order of 10^0, and thus dispersion still has a significant effect on the fluid and pollutant

transport. Conversely, the values of Pe_{diff} suggest that the transport through media is highly advection-controlled, relative to molecular diffusion, under all scenarios, on the order of 10^4 to 10^5. The relative magnitudes show that $Pe_{disp} << Pe_{diff}$, thus mechanical dispersion dominates the overall hydrodynamic dispersion and the effects molecular diffusion can be neglected in scaling up the sorption media reactor

Table 4.2. Dispersive (Pe_{disp}) and Diffusive (Pe_{diff}) Péclet number for the column scenarios

HRT (min)	q (cm·min^{-1})	u (cm·s^{-1})	Pe_{disp}	Pe_{diff}
12	2.49	0.039	4.9	$1.6*10^5$
18	1.66	0.026	9.2	$1.0*10^5$
24	1.24	0.020	7.7	$8.0*10^4$
30	1.00	0.015	5.0	$6.1*10^4$
39	0.77	0.012	8.9	$4.9*10^4$

If molecular diffusion is neglected, then the hydrodynamic dispersion coefficient reduces to longitudinal dispersion only, as was presented in 4.2.2, such that $D_h = \alpha_T u$. Figure 4.5 confirms this relationship for the data obtained from the tracer tests. It can be seen that a linear relationship does exist, where the slope of the line represents α_T. The deviation from perfect linearity can be contributed to random experimental error during the tracer tests. This is also exhibited in the variation of Pe_{disp}, which should theoretically be constant across each column scenario, but exhibited some variability. Establishing this relationship is key in the scaling process, as will be demonstrated in 4.3.4.
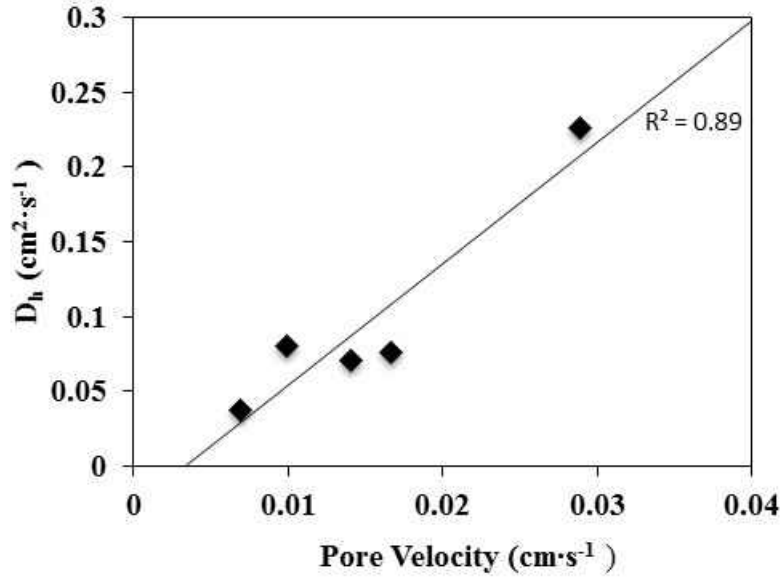
Figure 4.5. Linear dependence of the hydrodynamic dispersion coefficient, D_h on the pore velocity, u.

4.3.3. *Damköhler Number Calculations*

The Damköhler number was calculated for each of the 5 column scenarios and the results are presented in Table 4.3. Damköhler number (Da) for the 5 column scenarios. For all HRTs, it can be seen that the transport of copper is reaction-controlled, although only slightly. The observed range of Damköhler numbers was quite small, over a range much less than an order of magnitude. However, it still be clearly seen that the highest adsorptive capacity of 0.25 mg·g⁻¹ occurred at a Damköhler number of 2.74, with significant decreases in adsorptive capacity at slightly lower values ($q_0 = 0.033$ mg·g⁻¹ at $Da = 2.05$) and slightly higher values ($q_0 = 0.021$ mg·g⁻¹ at $Da = 0.3.42$). This reveals that the removal efficiency of the media is very sensitive to changes in the Damköhler number and only a very small range can produce the optimal environment for copper removal in the media (Figure 4.6).

Table 4.3. Damköhler number (Da) for the 5 column scenarios

HRT (min)	q (cm·min^{-1})	Da
12	2.49	1.37
18	1.66	2.05
24	1.24	2.74
30	1.00	3.42
39	0.77	4.45
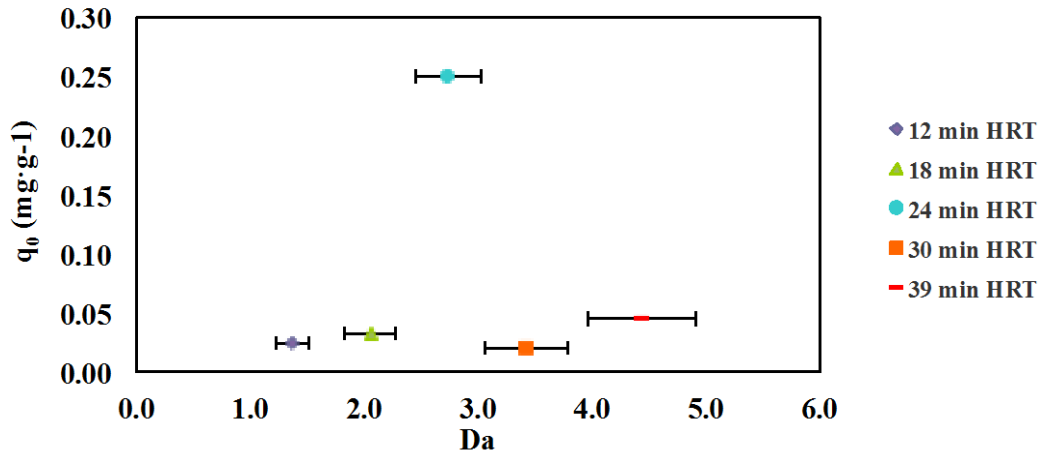
Figure 4.6. Relationship of equilibrium sorption capacity, q_0, to the Damköhler and Péclet numbers for the column tests. The error bars represent the range of Damköhler numbers calculated based on the standard deviation of the media bed length, l.

4.3.4. *Scaling-up from Laboratory to Field Scale Using Dimensionless Numbers*

As previously mentioned, the established scaling method presented Crittenden *et al.* (1986) is based on the dispersed-flow pore and surface diffusion model (DFPSDM) and provides similitude for the 6 independent dimensionless numbers that result from the DFPSDM. These numbers are summarized and defined in Table 4.4. However, it is not applicable for scaling reactors using unprocessed green sorption media, such as the mixture used in this study, as it relies on varying the media particle size between the lab and field-scale reactors. Therefore, development of an alternative method is desired for scaling of sorption media reactors using a constant media particle size.

83

Table 4.4. Summary and definition of dimensionless numbers that describe adsorbate transport under the DFPSDM and advection-dispersion-reaction governing equations.

Governing Equation	Dimensionless Number	Definition
Dispersed-Flow Pore and Surface Diffusion Model (DFPSDM)	Surface Solute Distribution Parameter (Dg_s)	$\dfrac{\text{Mass of Solute in Solid Phase}}{\text{Mass of Solute in Liquid Phase}}\Big|_{equilibrium}$
	Pore Solute Distribution Parameter (Dg_p)	$\dfrac{\text{Mass of Solute in Solid Phase}}{\text{Mass of Solute in Liquid Phase}}\Big|_{equilibrium}$
	Surface Diffusion Modulus (Ed_s)	$\dfrac{\text{Intraparticle Surface Diffusion Transfer Rate}}{\text{Advective Tranpsort Rate}}$
	Pore Diffusion Modulus (Ed_p)	$\dfrac{\text{Intraparticle Surface Diffusion Transfer Rate}}{\text{Advective Tranpsort Rate}}$
	Stanton (St)	$\dfrac{\text{Solute Liquid-Phase Mass Transfer Rate}}{\text{Advective Transport Rate}}$
	Péclet (Pe)	$\dfrac{\text{Advective Transport Rate}}{\text{Dispersive Transport Rate}}$
Advection-Dispersion-Reaction Equation	Damköhler (Da)	$\dfrac{\text{Surface Reaction Rate}}{\text{Advective Transport Rate}}$
	Péclet (Pe)	$\dfrac{\text{Advective Transport Rate}}{\text{Dispersive Transport Rate}}$

To overcome this issue, an alternative scaling method is presented based on the advection-dispersion equation. If the equation is extended to include an adsorptive reaction term (Lasaga, 1998), then two independent dimensionless numbers result that fully define the phenomenon: the Péclet number, and the Damköhler number. If the quantities of these numbers for the lab-scale column are equal to those of the full-scale reactor, then complete similitude is maintained. With the constant particle size approach necessary with green sorption media, the independent variables are reduced to hydraulic loading rate (q) and the fixed-bed length (l). The simplified relationships between the lab-scale, denoted by the subscript *LS* and field-scale, denoted by the subscript *FS* are shown in equations (33) and (34). Note that in (33), only longitudinal mechanical dispersion is considered for D_h.

$$Da_{LS} = Da_{FS} \Rightarrow \frac{C_0^{p-1}kl_{LS}}{q_{LS}} = \frac{C_0^{p-1}kl_{FS}}{q_{FS}} \Rightarrow \frac{l_{LS}}{q_{LS}} = \frac{l_{FS}}{q_{FS}} \tag{32}$$

$$Pe_{LS} = Pe_{FS} \Rightarrow \frac{u^2_{LS}\tau_{LS}}{D_h} = \frac{u^2_{FS}\tau_{FS}}{D_h} \Rightarrow \frac{u^2_{LS}\frac{V_{LS}}{Q_{LS}}n}{\alpha_L u_{LS}} = \frac{u^2_{FS}\frac{V_{FS}}{Q_{FS}}n}{\alpha_L u_{FS}} \Rightarrow$$

$$\frac{\frac{q_{LS}}{n}\frac{l_{LS}A_{LS}}{q_{LS}A_{LS}}n}{\alpha_L} = \frac{\frac{q_{FS}}{n}\frac{l_{FS}A_{FS}}{q_{FS}A_{FS}}n}{\alpha_L} \Rightarrow l_{LS} = l_{FS} \tag{33}$$

Examining the relationships, it can be seen that by adjusting q and l, perfect similitude cannot be maintained, if particle size remains constant between scales. As a result, the concept of partial similitude presented by Van Geem *et al*. (2007) must be applied in this situation. The results in 4.2.3 suggest that the removal efficiency is sensitive to changes in the Damköhler number, thus it is imperative that similitude be maintained for the reaction rate/advection rate relationship. As a result, the hydrodynamic similitude must be relaxed for scaling to occur, resulting in Péclet numbers that do not equate between lab and field scale. For highly advective (Pe >>1) or dispersive (Pe<<1) regimes, such a relaxation is not critical. However, for the observed results from this study, the values for the Péclet number are close to unity, thus large relaxation in hydrodynamic similarity would result in discrepancies between the lab and field-scale. A brief sensitivity analysis would illustrate that for a lab scenario of $Da = 1$ and $Pe = 10$, a tenfold increase in fixed bed length and hydraulic loading rate would result in $Da = 1$ and $Pe = 100$ in the field scale. An order magnitude change in the Péclet from lab to field scale could result in significant discrepancies, as the effect hydrodynamic dispersion would be greatly reduced relative to the advective velocity. Maintaining the Péclet number within the same order of magnitude between lab and field scale would ensure that major deviations in adsorptive capacity and breakthrough profile do not occur. Future work would call for a sensitivity analysis to determine the appropriate upper limit of a scalar increase in

the Péclet number from lab to field scale necessary for maintaining consistency between the expected and observed field performance, in terms of adsorption capacity and breakthrough profile.

4.4. <u>References</u>

Crittenden, J.C., J.K. Berrigan, J.K., and D.W. Hand. 1986. Design of rapid small-scale adsorption tests from constant diffusivity. *J. of Water Pollut. Control Federation* 58: 312-319.

Corwin, C.J., and R. Scott Summers. 2010. Scaling trace organic contaminant adsorption by granular activated carbon. *Environ. Sci. Technol.* 44: 5403-5408.

Cummings, L. and R. Scott Summers. 1994. Using RSSCTs to predict field-scale GAC control of DBP formation. *American Water Works Assoc.* 86: 88-97.

DeLima, S.A., Murad, M.A., Moyne, C., and D. Stemmelen. 2010. A three-scale model of pH-dependent flows and ion transport with equilibrium adsorption in kaolinite clays: I homogenization analysis. *Transp. Porous Med.* 85:23-44.

Fredd, C.N., and H.S. Fogler. 1998. Influence of transport and reaction on wormhole formation in porous media. *AIChE J.* 44: 1933-1949.

Golfier, F., Zarcone, C., Bazin, B., Lenormand, R., Lasseux, D., and M. Quintard. 2002. On the ability of a Darcy-scale model to capture wormhole formation during the dissolution of a porous medium. *J. Fluid Mech.* 457: 213-254.

Kang, Q., Zhang, D., and S. Chen. 2003. Simulation of dissolution and precipitation in porous media. *J. Geophys Res.* 108(B10): DOI: 10.1029/2003JB002504.

Kang, Q., Lichtner, P.C., and D. Zhang. 2006. Lattice Boltzmann pore-scale model for multicomponent reactive transport in porous media, *J. Geophys. Res.* 111: B05203, doi:10.1029/2005JB003951.

Knappe, D., V. Snoeyink, Roche, P., Prados, M.J., and M.-M. Bourbigot. 1997. The effect of preloading on rapid small-scale column test predictions of atrazine removal by GAC adsorbers. *Wat. Res.* 31: 2899-2909..

Lasaga, A.C. 1998. "Kinetic Theory in Earth Sciences". Pp 256-267. Princeton University Press, Princeton, NJ.

Steefel, C.I. 2008. Geochemical kinetics and transport. In "Kinetics of Water-Rock Interaction" Eds. S.L. Brantley, J.D. Kubicki, and A.F. White. Pp 545-590. Springer, New York.

Weihermuller, L., Kasteel, R., Vanderborght, J., Simunek, J., and H. Vereecken. 2011. Uncertainty in pesticide monitoring using suction cups: Evidence from numerical simulations. *Vadose Zone J.* 10: 1287-1298.

Werner, D., Karapanagioti, H.K., and D. A. Sabatini. 2012. Assessing the effect of grain-scale sorption rate limitations on the fate of hydrophobic organic groundwater pollutants, *J. Contaminant Hydrology.* 129-130: 70-79.

Westerhoff, P., Highfield, D., Badruzzaman, M., and Y. Yoon. 2005. Rapid Small-Scale Column Tests for Arsenate Removal in Iron Oxide Packed Bed Columns. *J. Environ. Engineering.* 131: 262-271.

Pang, L., Goltz, M., and M. Close. 2003. Application of the method of temporal moments to interpret solute transport with sorption and degradation. *J. Contaminant Hydrology.* 60: 123-134.

Van Geem, K., Zadjlik, R., Reyniers, M.F., and G. Marin. 2007. Dimensional analysis for scaling up and down steam cracking coils. *Chemical Engineering J.* 134: 3-10.

CHAPTER 5: CONCLUSIONS

5.1. <u>Adsorption-Desorption Processes</u>

After evaluation under equilibrium conditions for copper adsorption, the media mixture and each of the components exhibited were well described by both the Langmuir and Freundlich model. The relative adsorptive capacities were found to be coconut coir>media mixture>expanded clay aggregate>tire chunk with a. Equilibrium results also showed that increasing contact time favored greater adsorption for the mixture and coconut coir. A peak equilibrium sorption capacity of 71.1 mg·g^{-1} was reached for the coconut coir with a 60 minute contact time and a pH of 7.0. Reaction kinetics for the media mixture and individual media showed that the media mixture and coconut coir exhibited pseudo second-order kinetics, while the expanded clay kinetics were best described by second-order kinetics derived from the rate law. The coconut coir also proved to be most effective at copper adsorption under dynamic conditions, with an adsorption capacity of 1.63 mg·g^{-1}, compared to 0.021 mg·g^{-1} for the mixture at an HRT of 30 minutes, with precipitation further augmenting the copper removal.

Screening of potential desorbing agents showed that the use of HCl as a desorbing agent had the greatest potential. Batch equilibrium tests using 0.1 M HCl revealed a Freundlich-type desorption isotherm, which was highly nonlinear and concave in nature. Kinetic desorption tests found that the Lagergren pseudo-second order kinetic model best described the data and that the reaction was a rapid one, with over 50% of desorption occurring within 30 seconds. Batch adsorption and desorption was carried out over 3 cycles, showing that the tire chunk and expanded clay experience severely decreased adsorption by the 3rd cycle, while the media mixture and coconut coir exhibited only a modest decrease in adsorption over the 3 cycles, pointing to their potential for use over multiple life cycles. The potential for media regeneration through the use of strong acids as a desorbing agent enhances the status of the mixture

and coconut coir as a green sorption media, by promulgating green chemistry concepts. These concepts are realized in the fact that the media can serve multiple life cycles, it can be disposed as untreated non-hazardous waste at the end of its life cycle, and the sorbed copper can be recovered via metal hydroxide precipitation, generating little waste.

5.2. <u>Material Characterization</u>

Macro-scale characteristics were measured using ASTM standard methods for aggregates. The testing revealed that the media and media mixtures are quite porous, with porosities ranging from 0.36 for the tire chunk to 0.48 for the coconut coir. A particle size distribution for the media mixture revealed a uniform gradation, even though it has a three-part composition, and large median particle size of 7.5 mm.

FE-SEM imaging on media before and after adsorption found a strong correlation between the porosity of the micro pore structure and the adsorptive capacity of the media. XRD analyses revealed that the crystalline structure of the expanded clay and media mixture was dominated by hexagonal-typed SiO_2 and monoclinic-typed Al_2O_3 structures, while the tire chunk and coconut coir were characterized by graphitic structures, all of which are known to contain numerous micro-pores and cavities suitable for sorption. XRD analysis on Cu-loaded coconut coir revealed diffraction peaks that indicate cupric oxide (CuO) as the primary adsorbed copper species, which were digested and washed out during the desorption process. FE-SEM imaging and XRD analyses revealed primarily surface sorption of CuO species onto the coconut coir, which were digested and washed out during the desorption process. Elemental analysis using EDS supported the conclusions from the equilibrium adsorption and desorption tests, revealing measureable. amounts of copper in the coconut coir and media mixture in the Cu-loaded media followed by partial desorption. FTIR analysis found that the functional groups contained in the media mixture were

primarily S-H, O-H, and C=O, while no significant effects on the surface chemistry were observed on any media type after the use of HCl as a desorbing agent.

5.3. <u>Scaling Assessment for Field Implementation</u>

A study was conducted that examined the relationship between the Damköhler and Péclet numbers and the copper adsorption efficiency on a green sorption media in order to identify the conditions required for optimal copper removal. A series of 5 column breakthrough tests at varying hydraulic retention times revealed a clear peak removal efficiency at the 24 minute retention time with an adsorptive capacity of $q_0 = 0.25$ mg·g^{-1}, which corresponded to a Damköhler number of 2.74. The sorption capacity of the media was quite sensitive to small changes in the Damköhler number, thus selection of the HRT for a sorption media reactor must be carefully selected to ensure the Damköhler is close to this value. Additionally, a method of scaling sorption media reactors from lab-scale to field scale with a constant particle size was presented through a dimensional analysis involving the Péclet and Damköhler numbers. The dimensional analysis reveals that if similitude for the Damköhler number is maintained, similitude for the Péclet cannot be maintained. As a result, scaling up the sorption media reactor so as to keep the Péclet number within the same order of magnitude would be necessary to provide comparable performance between the lab-scale and field-scale reactor. This has implications on the cost savings in conducting lab-scale evaluations, as the scale cannot be reduced too greatly. Thus, applications which require a larger amount of sorption media would require larger lab-scale columns field implementation of multiple smaller reactors in parallel to achieve desired pollutant reduction goals.

5.4. <u>Final Remarks</u>

Based on the equilibrium and dynamic adsorption studies, the coconut coir in isolation shows the best potential for copper removal in an upflow media filter and exhibits a higher adsorption capacity (1.63 mg·g^{-1}) in comparison with the media mixture (0.25 mg·g^{-1}), which confirms the first hypothesis However, the larger macro-pore sizes in the coconut coir matrix could pass a large amount of particulate matter, resulting in clogging and excessive head loss within the filter and reduced system reliability. Including a chamber of expanded clay or media mixture for screening of particulates could benefit the use of a coconut coir media filter. However, in a complex stormwater matrix, multiple adsorbates with varying affinities sorption media are competing for the adsorption sites, thus a single-media filter may not provide a robust treatment if removal of other constituents such as cadmium or arsenic is of interest in addition to copper. Use of the media mixture in a media filter would provide the most cost-effective option as the adsorption capacity and regeneration potential are adequate while the heterogeneous pore structure would provide screening of particulates, thereby reducing head loss in the system.

After the desorption step, recovery of the desorbed copper and its removal from the waste stream is essential, otherwise it becomes merely a displacement of pollution (Tassist et al., 2009). While methods of copper recovery from the desorbing solution were not addressed in this work, the desorbed copper in solution may be removed from the waste stream and recovered using a number of methods and technologies. These include reverse osmosis and nanofiltration (Al-Zoubi et al., 2010, Mullett et al., 2014), chemical synthesis (Zhang and Zhang, 2014), and precipitation (Chen et al, 2014, Xie et al., 2005). Tassist et al. (2009) also used electrolysis to recover copper and other metals from desorbent solution as an electrochemical deposit. Establishing an effective and low-cost copper recovery method in practice is essential in establishing filter media sorption as an economical and sustainable treatment process, decreasing the need for landfill or hazardous waste disposal of the copper-loaded media.

There is a great possibility for future work with the green sorption media that would have both practical engineering and scientific benefits. Quantification of head loss characteristics of the media mixture and individual media would benefit in design of a filter system. A pilot-scale column test using stormwater spiked with copper can provide a breakthrough curve that more closely resembles expected field conditions by taking complex interactions with other constituents into account. Further work can be conducted to establish the media's adsorptive characteristics with respect to other single component systems, such as arsenic, cadmium, or lead. Finally, experimental work in multicomponent sorption with 2- or 3-metal adsorbate solutions would provide valuable results and model validation in this growing body of knowledge.

This work concludes a unique, low-cost green sorption media mixture comprised of expanded clay aggregate, tire chunk, and coconut coir, or coconut coir alone with a particulate-removing filter as an effective media for copper removal in wet detention stormwater systems. Application of the media mixture as a stormwater BMP would include the media placement in a baffle-box filter in a wet detention outflow structure or in a pumped upflow media bed reactor that would circulate the water possibly with a solar-powered pump system.

5.5. <u>References</u>

Al-Zoubi, H., Rieger, A., Steinberger, P., Pelz, W., Hasender, R., and G. Hartel. 2012. Nanofiltration of acid mine drainage. *Desalinization and Water Treat*. 21: 148-161.

Chen, T., Yan, B., Lei, C., and X Xiao. 2014. Pollution control and metal resource recovery for acid mine drainage. *Hydrometallurgy.* 147-148: 112-119.

Mullett, M., Fornarelli, R., and D. Ralph. 2014. Nanofiltration of mine water: Impact of feed pH and membrane charge on resource recovery and water discharge. *Membranes*. 4: 163-180.

Tassist, A., Lounici, H., Belhocine, D., Khelifa, A., and N. Mameri. 2009. Removal and recovery of copper from aqueous solutions by *Streptomyces rimosus* biomass: Enhancement of regeneration by desorption-electrolysis coupling. *Desalinization and Water Treat.* 3: 210-216.

Zhang, Z.Y., Zhang, F.S., 2014. A green process for copper recovery from waste printed circuit boards. *Advanced Mater. Processing.* 878: 374-379.

APPENDIX A: STATISTICAL ANALYSES

Mixture Vs Tire Chunk:

	Estimate	Std. Error	t value	Pr(>|t|)
Time	-0.01492	0.002661	-5.607	7.977e-07
MediaTire Chunk	0.8476	0.3058	2.772	0.00771
Time:MediaTire Chunk	-0.4191	0.05214	-8.038	1.108e-10
(Intercept)	0.03194	0.1921	0.1663	0.8686

Table: Fitting linear model: y ~ Time * Media

Mixture Vs Expanded Clay:

	Estimate	Std. Error	t value	Pr(>|t|)
Time	-0.6493	0.08146	-7.971	3.797e-10
MediaMixture	-1.08	0.4607	-2.345	0.0235
Time:MediaMixture	0.6344	0.0815	7.784	7.129e-10
(Intercept)	1.112	0.4177	2.663	0.01071

Table: Fitting linear model: y ~ Time * Media

Mixture Vs Coconut Coir:

	Estimate	Std. Error	t value	Pr(>|t|)
Time	-0.009868	0.0008033	-12.28	3.07e-19
MediaMixture	-2.09	0.1972	-10.6	2.848e-16
Time:MediaMixture	-0.005052	0.002303	-2.193	0.03157
(Intercept)	2.122	0.1209	17.56	1.537e-27

Table: Fitting linear model: y ~ Time * Media

Tire Chunk Vs Expanded Clay:

	Estimate	Std. Error	t value	Pr(>|t|)
Time	-0.6493	0.09642	-6.734	3.913e-08
MediaTire Chunk	-0.2326	0.5705	-0.4076	0.6857
Time:MediaTire Chunk	0.2153	0.1148	1.875	0.06797
(Intercept)	1.112	0.4944	2.25	0.0299

Table: Fitting linear model: y ~ Time * Media

Tire Chunk Vs Coconut Coir:

	Estimate	Std. Error	t value	Pr(>|t|)
Time	-0.009868	0.0009328	-10.58	6.248e-16
MediaTire Chunk	-1.243	0.2644	-4.699	1.342e-05
Time:MediaTire Chunk	-0.4242	0.04907	-8.645	1.659e-12
(Intercept)	2.122	0.1404	15.12	2.793e-23

Table: Fitting linear model: y ~ Time * Media

Expanded Clay Vs Coconut Coir:

	Estimate	Std. Error	t value	Pr(>|t|)
Time	-0.009868	0.000935	-10.55	2.673e-15
MediaExpanded Clay	-1.01	0.4145	-2.437	0.01781
Time:MediaExpandedClay	-0.6394	0.07605	-8.408	9.91e-12
(Intercept)	2.122	0.1407	15.08	4.414e-22

Table: Fitting linear model: y ~ Time * Media

12 min vs 18 min HRT

	Estimate	Std. Error	t value	Pr(>|t|)
Time	-0.1146	0.0124	-9.242	4.532e-13
HRT18	0.5751	0.3411	1.686	0.09703
Time:HRT18	0.01791	0.0183	0.9788	0.3317
(Intercept)	0.8646	0.2251	3.841	0.0003014

Table: Fitting linear model: y ~ Time * HRT

12 min vs 24 min HRT

	Estimate	Std. Error	t value	Pr(>|t|)
Time	-0.1146	0.01094	-10.48	2.365e-15

97

```
  **HRT24**      0.4191    0.2704    1.55     0.1263
 **Time:HRT24**   0.106    0.01103    9.607  6.874e-14
 **(Intercept)**  0.8646    0.1985    4.356  5.062e-05
-----------------------------------------------------------
```
Table: Fitting linear model: y ~ Time * HRT

12 min vs 30 min HRT
```
----------------------------------------------------------
          Estimate  Std. Error  t value  Pr(>|t|)
---------------- ---------- ------------ --------- ----------
  **Time**      -0.1146    0.01204    -9.515  1.603e-13
  **HRT30**     -0.8327    0.304     -2.739   0.008137
 **Time:HRT30**  0.09968   0.01239    8.042   4.647e-11
 **(Intercept)**  0.8646    0.2186    3.955   0.0002078
----------------------------------------------------------
```
Table: Fitting linear model: y ~ Time * HRT

12 min vs 39 min HRT
```
----------------------------------------------------------
          Estimate  Std. Error  t value  Pr(>|t|)
---------------- ---------- ------------ --------- ----------
  **Time**      -0.1146    0.0119    -9.628   1.643e-14
  **HRT39**     -0.01352   0.2763   -0.04892  0.9611
 **Time:HRT39**  0.1003    0.01201    8.348   3.791e-12
 **(Intercept)**  0.8646    0.2161    4.002   0.0001524
----------------------------------------------------------
```

Table: Fitting linear model: y ~ Time * HRT

18 min vs 24 min HRT
```
----------------------------------------------------------
          Estimate  Std. Error  t value  Pr(>|t|)
---------------- ---------- ------------ --------- ----------
  **Time**      -0.09668   0.009027   -10.71  1.849e-15
  **HRT24**     -0.156     0.2214    -0.7047  0.4838
 **Time:HRT24**  0.08807   0.009096   9.683   8.489e-14
 **(Intercept)**  1.44      0.1718    8.379   1.255e-11
----------------------------------------------------------
```

18 min vs 30 min HRT
```
----------------------------------------------------------
```

```
         Estimate   Std. Error   t value   Pr(>|t|)
---------------- ---------- ------------ --------- ----------
  **Time**      -0.09668    0.01049     -9.22    7.972e-13
  **HRT30**      -1.408      0.2618     -5.377   1.528e-06
 **Time:HRT30**  0.08176    0.01075      7.609   3.411e-10
 **(Intercept)**   1.44      0.1996      7.213   1.538e-09
-----------------------------------------------------------
```
Table: Fitting linear model: y ~ Time * HRT

18 min vs 39 min HRT
```
---------------------------------------------------------------
            Estimate   Std. Error   t value   Pr(>|t|)
---------------- ---------- ------------ --------- ----------
  **Time**      -0.09668    0.0108      -8.955   4.067e-13
  **HRT39**      -0.5886     0.2509     -2.346   0.02189
 **Time:HRT39**  0.08237    0.01088      7.57    1.324e-10
 **(Intercept)**   1.44      0.2055      7.006   1.384e-09
---------------------------------------------------------------
```
Table: Fitting linear model: y ~ Time * HRT

24 min vs 30min HRT
```
---------------------------------------------------------------
            Estimate    Std. Error   t value   Pr(>|t|)
---------------- ---------- ------------ --------- ----------
  **Time**      -0.008615   0.001039    -8.288   1.783e-11
  **HRT30**       -1.252     0.1888      -6.63    1.141e-08
 **Time:HRT30**  -0.006305   0.002156    -2.925   0.004888
 **(Intercept)**   1.284     0.1306       9.83    4.863e-14
---------------------------------------------------------------
```
Table: Fitting linear model: y ~ Time * HRT

24 min vs 39 min HRT
```
---------------------------------------------------------------
            Estimate    Std. Error   t value   Pr(>|t|)
---------------- ---------- ------------ --------- ----------
  **Time**      -0.008615   0.001129    -7.628   8.167e-11
  **HRT39**      -0.4326     0.1873      -2.31    0.02382
 **Time:HRT39**  -0.005696   0.001617    -3.523   0.0007501
 **(Intercept)**   1.284     0.1419       9.047   1.919e-13
---------------------------------------------------------------
```
Table: Fitting linear model: y ~ Time * HRT

30 min vs 39 min HRT

	Estimate	Std. Error	t value	Pr(>|t|)
Time	-0.01492	0.002322	-6.426	1.51e-08
HRT39	0.8192	0.2173	3.769	0.0003452
Time:HRT39	0.000609	0.002665	0.2285	0.8199
(Intercept)	0.03194	0.1676	0.1905	0.8494

Table: Fitting linear model: y ~ Time * HRT

APPENDIX B: PÉCLET AND DAMKÖHLER CALCULATIONS

The Péclet numbers for dispersion and diffusion were calculated using the following relations:

$$Pe_{Disp} = \frac{u^2 \tau}{D_h}$$

$$Pe_{Diff} = \frac{ul}{D_m}$$

where u (cm·s^{-1}) is the interstitial velocity, defined as the flow rate per unit area divided by the porosity, τ (s) is the residence time in the system, D_h (cm^2·s^{-1}) is the hydrodynamic dispersion coefficient, l is the characteristic length scale which is taken to be the average fixed-bed length from the column study, and D_m is the molecular diffusion coefficient which is taken to be $7.33*10^{-6}$ cm^2·s^{-1} for Cu^{2+} (Lasaga, 1998).

The interstitial velocity was calculated as:

$$u = \frac{Q}{A} \cdot \frac{1}{n}$$

where Q was the calibrated flow rate during the column study (mL·s^{-1}), A is the measured cross-sectional area of the column (22.9 cm^2), and n was the porosity, a determined using ASTM standard D854-92 to be 0.38 for the media mixture.

The length of the fixed bed was kept at a constant 35.8 cm for all tracer tests. It should be noted that while compaction varied between successive tracer tests, a constant porosity was assumed for each test. Additionally, the theoretical residence time for the tracer test differed from the residence time associated with the column adsorption test, since different size columns were used, but the theoretical interstitial velocity was kept constant, since it is a squared term and has a larger effect on the theoretical Péclet number. A summary of the Péclet numbers and the associated variables and parameters is summarized in the table below:

Column Scenario (HRT, min)	Q (mL·s⁻¹)	Porosity	τ (s)	l (cm)	u (cm·s⁻¹)	D_m (cm²·s⁻¹)	D_h (cm²·s⁻¹)	Pe_{Disp}	Pe_{Diff}
12	0.43	0.38	720	35.8	0.039	$7.33*10^{-6}$	0.23	4.7	$1.6*10^5$
18	0.28	0.38	1080	35.8	0.026	$7.33*10^{-6}$	0.076	9.2	$1.0*10^5$
24	0.22	0.38	1440	35.8	0.020	$7.33*10^{-6}$	0.071	7.8	$8.0*10^4$
30	0.17	0.38	1800	35.8	0.015	$7.33*10^{-6}$	0.081	5.0	$6.1*10^4$
39	0.13	0.38	2340	35.8	0.012	$7.33*10^{-6}$	0.038	8.9	$4.9*10^4$

The Damköhler number was calculated using the following relation:

$$Da = \frac{C_0^{p-1}kl}{q}$$

where k is the reaction rate constant, C_0 (mg·L⁻¹) is the influent concentration, p is order of reaction (dimensionless), l (cm) is the fixed-bed length from the column study and q (cm·min⁻¹) is the hydraulic loading rate.

To calculated the average Damköhler number, the fixed bed length, l (cm) was taken to be the average of three measurements, and the estimated high and low Damköhler numbers were calculated using the standard deviation of the fixed bed length. This was done to account for the varying compaction during column preparation, since a constant mass of media was used between triplicate columns for the breakthrough study, instead of a constant bed length as was used in the tracer study. It should be noted that while compaction varied between columns, a constant porosity was assumed throughout. The hydraulic loading rate, q is synonymous with the interstitial velocity. A summary of the Damköhler numbers and the associated variables and parameters is summarized in the table below:

Column Scenario (HRT, min)	Q (mL·min⁻¹)	Porosity	l (cm)	q (cm·min⁻¹)	p	k (L·mg⁻¹·min⁻¹)	C_o (mg·L⁻¹)	Da
12	26	0.38	29.9±3.2	2.49	2	0.114	1.0	1.37
18	17	0.38	29.9±3.2	1.66	2	0.114	1.0	2.05
24	13	0.38	29.9±3.2	1.24	2	0.114	1.0	2.74

30	10	0.38	29.9±3.2	1.00	2	0.114	1.0	3.42
39	8	0.38	29.9±3.2	0.77	2	0.114	1.0	4.45

Lasaga, A.C. 1998. "Kinetic Theory in Earth Sciences". Pp 256-267. Princeton University Press,

Princeton, NJ.